Theory of the lattice Boltzmann method: Acoustic and thermal properties in two and three dimensions

Pierre Lallemand[1,*] and Li-Shi Luo[2,†]

[1]*Laboratoire ASCI, Bâtiment 506, Université Paris-Sud (Paris XI Orsay), 91405 Orsay Cedex, France*
[2]*ICASE, MS 132C, NASA Langley Research Center, 3 West Reid Street, Building 1152, Hampton, Virginia 23681-2199, USA*

The focus of the present work is to provide an analysis for the acoustic and thermal properties of the energy-conserving lattice Boltzmann models, and a solution to the numerical defects and instability associated with these models in two and three dimensions. We discover that a spurious algebraic coupling between the shear and energy modes of the linearized evolution operator is a defect universal to the energy-conserving Boltzmann models in two and three dimensions. This spurious mode coupling is highly anisotropic and may occur at small values of wave number k along certain directions, and it is a direct consequence of the following key features of the lattice Boltzmann equation: (1) its simple spatial-temporal dynamics, (2) the linearity of the relaxation modeling for collision operator, and (3) the energy-conservation constraint. To eliminate the spurious mode coupling, we propose a hybrid thermal lattice Boltzmann equation (HTLBE) in which the mass and momentum conservation equations are solved by using the multiple-relaxation-time model due to d'Humières, whereas the diffusion-advection equation for the temperature is solved separately by using finite-difference technique (or other means). Through the Chapman-Enskog analysis we show that the hydrodynamic equations derived from the proposed HTLBE model include the equivalent effect of $\gamma = C_P/C_V$ in both the speed and attenuation of sound. Appropriate coupling between the energy and velocity field is introduced to attain correct acoustics in the model. The numerical stability of the HTLBE scheme is analyzed by solving the dispersion equation of the linearized collision operator. We find that the numerical stability of the lattice Boltzmann scheme improves drastically once the spurious mode coupling is removed. It is shown that the HTLBE scheme is far superior to the existing thermal LBE schemes in terms of numerical stability, flexibility, and possible generalization for complex fluids. We also present the simulation results of the convective flow in a rectangular cavity with different temperatures on two opposite vertical walls and under the influence of gravity. Our numerical results agree well with the pseudospectral result.

I. INTRODUCTION

In spite of its success in solving various challenging flow problems involving athermal (or isothermal) fluids, the lattice Boltzmann equation (LBE) has not been able to handle realistic thermal (and fully compressible) fluids with satisfaction. Even though there has been a continuous endeavor in this area for obvious reasons [1–36], the prospect of applying the lattice Boltzmann method to thermo-hydrodynamics is not yet entirely clear. From a practical point of view, the application of the thermal lattice Boltzmann equation (TLBE) is hampered by numerical instabilities when the local velocity of the flow increases. Even though the equations for mass, momentum, and energy-conservation laws can be derived from some existing LBE models, the numerical stability of the existing TLBE models is often confined to such a narrow region in the parameter space of the transport coefficients and to such small velocities that the LBE simulations are limited to flows of relatively small Reynolds numbers. This poses a severe limitation on TLBE schemes for realistic applications of computational fluid dynamics (CFD).

To appreciate what has been accomplished so far and to place the present work in perspective, we begin with a concise review of existing work on thermal and compressible lattice Boltzmann schemes. We classify the existing TLBE models into three categories. The first category, which is also the simplest approach, is that of passive scalar [2–6]. In this approach, the temperature is treated as a passive scalar, which is advected by the flow velocity but does not affect the flow fields (density and velocity). The flow fields and the passive-scalar temperature are represented by two sets of distribution functions: one simulates the Navier-Stokes equation, and the other simulates the advection-diffusion equation satisfied by the passive scalar driven by the flow [2–5]. Numerically, this is not very efficient because there is no need to use a full set of distribution functions to simulate a passive scalar, even though this numerical inefficiency can be improved somewhat by using some redundant degree of freedom in some LBE models [6]. The limitation of this approach is obvious, and we shall have no further discussion of it.

The second category of the TLBE models includes various shock capturing schemes based on the lattice Boltzmann method to treat fully compressible Euler [7–9] or Navier-Stokes [10–15] equations. The existing LBE Euler schemes are constructed in several ways. The first approach uses an interpolated advection such that the viscous term can be canceled out in the leading order of the Taylor expansion for the

*Electronic address: lalleman@asci.fr
†Present address: National Institute of Aerospace, 144 Research Drive, Hampton, VA 23666. Electronic address: luo@NIAnet.org; URL: http://research.nianet.org/~luo

distribution function [8]. The second one solves the discrete velocity model of the Boltzmann equation by a finite-difference scheme [9]. It should be noted that the equilibrium distribution functions in all these LBE Euler schemes are polynomials of hydrodynamic variables: density, velocity, and internal energy (or temperature), and therefore the Mach number cannot be too large. There are also several LBE models for the compressible thermal Navier-Stokes equations [10–15]. In order to allow large speeds, the advection step is adapted to the local flow velocity [37], thus it is no longer a simple process of hopping from one grid point to the next, and interpolations have to be used. Interpolation can introduce undesirable numerical artifacts which can affect small scale details, and thus its effects in the LBE method need to be considered more carefully. The equilibrium can be a polynomial [10] or other more complicated algebraic functions [11], or a Kronecker δ function that helps to increase the Mach number [12–14]. (This approach is, in fact, related to the beam scheme [38,39].) Another approach is to use a large set of discrete velocities with a set of distribution functions of Maxwellian form for particle number density and another for particle energy density [15]. This scheme effectively doubles the number of discrete velocities and is implicit [15]. It is important to note that the numerical analysis for the LBE shock capturing schemes is yet to be done—the numerical accuracy of these schemes remains by and large unknown. It is not clear what benefit these schemes can offer especially when there are other more mature shock capturing schemes based on kinetic theory (cf. Refs. [40,41] and references therein). We shall not further discuss the LBE models in the second category because it is beyond the scope of the present work.

The third category of the TLBE models corresponds to their athermal counterparts with energy-conservation constraint and possibly other modifications. To the best of our knowledge, most energy-conserving TLBE models in this third category are characterized by low (or moderate at best) Mach number and Boussinesq approximations. The essence of Boussinesq approximation is that the density variation only appears in the forcing term (the buoyancy force), and all the transport coefficients (viscosities and heat conductivity) and the sound speed are (almost) independent of temperature. There has been a number of proposals to make the energy-conserving lattice Boltzmann equation capable of simulating thermohydrodynamics.

(1) To increase the number of velocities [16,18], and to include higher-order nonlinear terms (in flow velocity) in the equilibrium distribution functions [19].

(2) To use equilibrium distribution functions depending on variable temperature [7,16,17].

(3) To implement an advection with finite-difference schemes, such as the Lax-Wendroff scheme, to improve numerical stability by increasing numerical dissipations [20,21].

(4) To use two sets of distribution functions for particle number density, and energy density, which effectively doubles the number of discrete velocities [22–25]. This is based on a linearization of temperature dependence of the distribution functions and the fact that the Gaussian quadra-

tures associated with the LBE models can preserve the energy and heat flux exactly [42–44].

(5) To use a velocity set of better symmetry, which does not naturally coincide with a lattice structure in physical space [27–31]. Interpolations in physical space must be used in this case, and these schemes [27–31] are no longer conservative—interpolations destroy local conservation laws. Often the symmetry of the spatial interpolations used in these schemes differs from that of the discrete velocity set, thus the anisotropic nature of these interpolations can dictate the isotropic property of these schemes regardless the symmetry of the discrete velocity set. In addition, interpolations can increase numerical dissipation, particularly on small scales comparable to the size of grid spacing (cf. Appendix G and Ref. [45]).

(6) To use energy-dependent discrete velocities [32]. In this case, interpolations in velocity space must be applied in addition to spatial interpolations. Specifically, because the directions of discrete velocities are fixed, the interpolations must consider energy variations. This may exacerbate numerical dissipation and other artifacts due to spatial interpolations, and the scheme [32] is no longer conservative. These numerical artifacts can be much more severe than in the case with spatial interpolations only [46], and are particularly strong in small scales comparable to the size of grid spacing (cf. Appendix G).

(7) To use a hybrid scheme in which the flow simulation is decoupled from the solution of the temperature equation. Specifically, the flow simulation is accomplished by using the lattice Boltzmann equation, while the temperature equation is solved by using finite-difference schemes [33,34] or other means [35].

In spite of all the effort, the success of the thermal lattice Boltzmann equation is still rather limited in the sense that it is not yet as competitive as the athermal lattice Boltzmann equation, and it cannot perform as well as traditional CFD methods in many aspects. As it has been noticed previously, the main difficulty the thermal lattice Boltzmann equation faces is the numerical instability. Although there are some discussions of the numerical instability in the TLBE schemes [1,18,20,28,36], so far the true nature of the numerical instability is still not well understood.

It is the aim of this work to first present a systematic analysis of the defects and numerical instability of the TLBE schemes, and then to propose an approach to eliminate these defects and to improve the numerical stability. The scope of this work is limited to the TLBE schemes for low (or possibly moderate) Mach number flows. The hydrodynamic system considered here has correct mass and momentum conservation equations and correct acoustics. However, we do not include nonlinear dissipation terms in the temperature equation for two reasons. First, these terms are not important for acoustics (which is the focus of the present work), and second, they are, in fact, negligible for nearly incompressible fluids [35,47]. Our analysis begins with a comparative analysis of athermal and thermal lattice Boltzmann equations. We find that a very severe defect of the energy-conserving lattice Boltzmann models is the spurious algebraic coupling between the viscous mode and the energy mode of the linear-

ized evolution operator of the system (cf. Appendix B).

The location in k-space where this spurious coupling takes place is highly anisotropic and can occur at a very small value of k or on a continuous range of k along certain directions, and it depends on the Prandtl number Pr. Also, the energy-conserving TLBE models are prone to numerical instabilities, which can be instigated by fluctuations of a wide-ranged scale. In contrast, for the athermal LBE models a similar coupling occurs only when the wave number k is near π, making the athermal LBE models only sensitive to the small scale fluctuations. Hence the athermal LBE models can be extremely stable if small scale fluctuations are carefully dealt with [45]. We also observe that the spurious mode coupling between the energy and shear modes cannot be removed by increasing the number of discrete velocities—it is intrinsic to the simplicity of the spatial-temporal evolution of the lattice Boltzmann equation. To overcome this difficulty, we propose a hybrid lattice Boltzmann equation in which the mass and momentum conservation laws are solved by the usual athermal lattice Boltzmann equation, while the advection-diffusion equation satisfied by the temperature is solved separately by finite-difference technique (or by other means). In this approach the energy-conservation law is decoupled from the mass and momentum conservation laws, and therefore the spurious mode coupling is removed. In addition to the improvement of numerical stability, the proposed hybrid TLBE (HTLBE) method is numerically efficient because it uses less degrees of freedom than energy-conserving TLBE models.

Since in the present work we adopt the strategy of a hybrid lattice Boltzmann method which has been advocated previously [33,34], it is imperative to point out the differences between the method proposed in the present work and the existing one. First and foremost, we use the multiple-relaxation-time (MRT) collision model due to d'Humières [1,45,49,50] and abandon the popular single-relaxation-time model due to Bhatnagar, Gross, and Krook (BGK) [51], i.e., the lattice BGK model. We shall demonstrate that the lattice BGK model (LBGK) is intrinsically inferior to the MRT model, and it is largely responsible for numerical instabilities observed in the TLBE simulations. Second, because of the MRT model, appropriate coupling between the temperature, mass, and momentum can be easily accomplished, and this is not possible for the lattice BGK models. Specifically, the ratio of specific heats ($\gamma = C_P/C_V$) in the proposed scheme is an adjustable parameter, as opposed to a fixed constant in the previous ones [33,34]. We do not explicitly use the Boussinesq approximation, and thus are able to consider temperature-dependent transport coefficients and other effects. Third, the finite-difference stencils used for the temperature equation in the present work are uniquely determined by the dispersion equation analysis to optimize the linear stability of the system. And fourth, we avoid using interpolations in the proposed TLBE scheme. Because the finite-difference stencils used for the temperature equation have the same symmetries as the underlying discrete velocity set in the model, the isotropy determined by the discrete velocity set remains intact. With the above new features, the proposed TLBE scheme can significantly enhance the numerical stability.

The remaining part of the paper is organized as follows. Section II reviews the athermal lattice Boltzmann models without the energy-conservation constraint. These models are studied within the MRT-LBE framework (or the moment method) [1,45,49,50]. Through the analysis of the linearized dispersion equation [45], constraints on various parameters in the equilibria of nonconserved moments are obtained. Section III studies the lattice Boltzmann models with the energy-conservation constraint. The analysis of the linearized dispersion equation is applied to the energy-conserving lattice Boltzmann models. Transport coefficients and the sound speed are determined for various models in two and three dimensions. Based on the linear analysis, we conclude that, due to a spurious mode coupling and numerical instabilities which can be instigated by fluctuations of wide-ranged scales, the energy-conserving lattice Boltzmann models (BGK or MRT models) are not suitable for numerical simulations. It is shown that the spurious mode coupling cannot be removed by increasing the number of discrete velocities. Based on analysis presented in Sec. III, Sec. IV proposes a hybrid TLBE scheme that uses the athermal lattice Boltzmann equation for the mass and momentum conservation laws, and solves the diffusion-advection equation for the temperature by using finite difference (or other techniques). The dispersion equation analysis is applied to the HTLBE schemes in two and three dimensions to ensure the (linear) stability. We observe that once the spurious coupling is removed, the numerical stability improves drastically. Section V presents simulations of the convective flow in a three-dimensional rectangular cavity with two opposite vertical walls at different temperatures by using the 13-velocity HTLBE model. Critical Nusselt number obtained by using the HTLBE scheme agrees well with the pseudospectral result. Finally, Sec. VI concludes the paper. Several appendixes provide technical details referred to in the text. Appendix A outlines the construction of the transformation matrix by using the D2Q9 (2-dimensional 9-velocity) model as an example. Appendix B gives a concise discussion on the dispersion equation analysis within LBE framework. Appendix C provides the finite-difference stencils for the gradient and the Laplacian operators for the D2Q9 model. Appendixes D–F provide the transformation matrices and the stencils for the gradient and the Laplacian operators for the D3Q13, D3Q15, and D3Q19 models in three dimensions, respectively. Finally, Appendix G studies the two-dimensional (2D) nine-velocity "octagonal" LBGK model [27–31] through the dispersion equation analysis and discusses the effects due to interpolations.

II. BRIEF REVIEW OF ATHERMAL LATTICE BOLTZMANN EQUATION

A. Multiple-relaxation-time lattice Boltzmann equation

There are three discretizations involved in the lattice Boltzmann equation: velocity space, physical space, and time discretizations, i.e., phase space and time discretizations. Moreover, these three discretizations are coupled together so

that the lattice Boltzmann equation has a very simple two-step spatial-temporal evolution consisting of collision and advection. The simplicity of the LBE dynamics has a drawback in terms of the numerical instability.

We consider the lattice Boltzmann equation as a fully discrete dynamical system evolving on a D-dimensional discrete lattice based on a set of $B = (b+1)$ discrete velocities,

$$\{\boldsymbol{c}_i | i = 0, \ldots, b\},$$

according to a set of rules which enforces the local conservation laws. With the discrete velocity set given, a set of B real numbers on each lattice point $\boldsymbol{r}_j$ and at a discrete time t_n,

$$\{f_i(\boldsymbol{r}_j, t_n) | i = 0, \ldots, b\},$$

is used to represent the discretized analog of the single-particle distribution function of a real gas. A column vector in phase space is denoted by a ''ket'' vector,

$$|f(\boldsymbol{r}_j, t_n)\rangle = (f_0(\boldsymbol{r}_j, t_n), f_1(\boldsymbol{r}_j, t_n), \ldots, f_b(\boldsymbol{r}_j, t_n))^{\mathsf{T}},$$

where T is the transpose operator. Without losing any information, $B \, (=b+1)$ number of distribution functions can be linearly mapped to an equal number of moments,

$$\{m_i(\boldsymbol{r}_j, t_n) | i = 1, 2, \ldots, (b+1)\},$$

i.e., the space $\mathbb{F} = \mathbb{R}^B$ spanned by $|f\rangle$ can be linearly mapped into another space $\mathbb{M} = \mathbb{R}^B$ spanned by

$$|m(\boldsymbol{r}_j, t_n)\rangle = (m_1(\boldsymbol{r}_j, t_n), m_2(\boldsymbol{r}_j, t_n), \ldots, m_{b+1}(\boldsymbol{r}_j, t_n))^{\mathsf{T}},$$

by an invertible linear mapping M such that

$$|m\rangle = \mathsf{M}|f\rangle, \quad |f\rangle = \mathsf{M}^{-1}|m\rangle.$$

In the setting of the generalized lattice Boltzmann equation or the moment method, as proposed by Ref. [1] and advocated by others [45,49,50], the lattice Boltzmann equation can be written as

$$|f(\boldsymbol{r}_j + \boldsymbol{c}_i, t_n + 1)\rangle = |f(\boldsymbol{r}_j, t_n)\rangle - \mathsf{M}^{-1}\mathsf{S}[|m(\boldsymbol{r}_j, t_n)\rangle$$
$$- |m^{(\text{eq})}(\boldsymbol{r}_j, t_n)\rangle], \quad (1)$$

where elements of the diagonal matrix S are relaxation rates $\{s_i | i = 1, 2, \ldots, (b+1)\}$, i.e.,

$$\mathsf{S} = \text{diag}(s_1, s_2, \ldots, s_{b+1}),$$

and $|m^{(\text{eq})}\rangle$ is the equilibrium-moment vector, the components of which are the equilibria of the moments [1,45,49,50]. Therefore, the collision step is executed in the

space $\mathbb{M}$ of moments, while the advection step is performed in the space $\mathbb{F}$ of distribution functions so that the relaxation rates for different nonconserved modes can be adjusted.

There are three elements in the above evolution equation: the linear mapping M, the equilibrium values of the moments $\{m_i^{(\text{eq})} | i = 1, 2, \ldots, (b+1)\}$, and the relaxation matrix S. The equilibria of the moments should depend only on the local values of the conserved moments (mass density, momentum, and energy for TLBE models). The values of the relaxation rates $\{s_i | i = 1, 2, \ldots, (b+1)\}$ in S are determined by a linear analysis [45].

For a given velocity set on symmetric lattices, the transformation matrix M can be easily constructed by applying the Gram-Schmidt orthogonalization procedure to monomials of Cartesian components of the discrete velocities $\{c_{ix}^m c_{iy}^n | m, n \geq 0\}$ in two dimensions (and $\{c_{ix}^l c_{iy}^m c_{iz}^n | l, m, n \geq 0\}$ in three dimensions) [1,45,49,50]. Appendix A discusses the construction of the transformation matrix M on symmetric 2D square lattices and 3D cubic lattices. (For asymmetric lattices, see Ref. [52].)

We note that the LBGK model is a special case of its MRT counterpart: by choosing a special set of parameter values in the equilibria of the moments and one single relaxation rate $s_i = 1/\tau$, the MRT LBE model reduces to the BGK model [45]. In the MRT setting, all modes are orthogonal and can be controlled individually. This therefore allows the MRT model to include the maximum number of adjustable parameters. The dispersion equation analysis (von Neumann analysis), as briefly discussed in Appendix B, can provide insights into hydrodynamic and nonhydrodynamic behaviors and the (linear) numerical stability of the underlying lattice Boltzmann model, and in turn determines the *linearly* optimal values of the adjustable parameters in the MRT model [45]. Because of the equivalence between the moment and discrete velocity representations, it is obvious that introducing more and more velocities means including moments of higher and higher orders, and therefore more and more adjustable parameters. We assume that a minimum number of discrete velocity is required by the underlying physics, and the choice of the velocity set affects the numerical properties of the model. The dispersion equation analysis can provide an understanding of the influence of the adjustable parameters on the ability of the model to simulate fluid flows—the parameters appear in the transport coefficients, the sound speed, and Galilean-invariance factor as functions of $\boldsymbol{k}$. We observe that beyond a certain number of degrees of freedom, adding higher order terms in the equilibria will not affect hydrodynamic behavior, even though this may help to improve stability and Galilean invariance. We will demonstrate this point through examples in what follows.

B. 13-velocity model on a 2D square lattice

We use a thirteen-velocity model with four speeds (0, 1, $\sqrt{2}$, and 2) on a two-dimensional square lattice (D2Q13S model) as an example. The labeling of the velocities is depicted in Fig. 1. The transformation matrix M for this model is

$$
\begin{pmatrix}
\langle\rho| \\
\langle j_x| \\
\langle j_y| \\
\langle e| \\
\langle p_{xx}| \\
\langle p_{xy}| \\
\langle\varepsilon| \\
\langle h| \\
\langle\pi_{xx}| \\
\langle q_x| \\
\langle\eta_x| \\
\langle q_y| \\
\langle\eta_y|
\end{pmatrix}
=
\begin{pmatrix}
1 & 1 & 1 & 1 & 1 & 1 & 1 & 1 & 1 & 1 & 1 & 1 & 1 \\
0 & 1 & 0 & -1 & 0 & 1 & -1 & -1 & 1 & 2 & 0 & -2 & 0 \\
0 & 0 & 1 & 0 & -1 & 1 & 1 & -1 & -1 & 0 & 2 & 0 & -2 \\
-28 & -15 & -15 & -15 & -15 & -2 & -2 & -2 & -2 & 24 & 24 & 24 & 24 \\
0 & 1 & -1 & 1 & -1 & 0 & 0 & 0 & 0 & 4 & -4 & 4 & -4 \\
0 & 0 & 0 & 0 & 0 & 1 & -1 & 1 & -1 & 0 & 0 & 0 & 0 \\
140 & -2 & -2 & -2 & -2 & -67 & -67 & -67 & -67 & 34 & 34 & 34 & 34 \\
-12 & 8 & 8 & 8 & 8 & -6 & -6 & -6 & -6 & 1 & 1 & 1 & 1 \\
0 & -4 & 4 & -4 & 4 & 0 & 0 & 0 & 0 & 1 & -1 & 1 & -1 \\
0 & -2 & 0 & 2 & 0 & -1 & 1 & 1 & -1 & 2 & 0 & -2 & 0 \\
0 & 4 & 0 & -4 & 0 & -3 & 3 & 3 & -3 & 1 & 0 & -1 & 0 \\
0 & 0 & -2 & 0 & 2 & -1 & -1 & 1 & 1 & 0 & 2 & 0 & -2 \\
0 & 0 & -4 & 0 & 4 & 3 & 3 & -3 & -3 & 0 & -1 & 0 & 1
\end{pmatrix}.
\tag{2}
$$

The row vectors in M (from top to bottom) correspond to the following moments: the mass density ρ (zeroth-order moment), and x and y components of momentum, j_x and j_y (first-order moment), the energy e (second-order moment), the components of the stress tensor $p_{xx}=(j_x^2-j_y^2)$ and $p_{xy}=j_x j_y$ (second-order moment), energy square $\varepsilon\propto e^2$ (fourth-order moment), energy cubic $h\propto e^3$ (sixth-order moment), a fourth-order moment $\pi_{xx}\propto e p_{xx}$, x component of heat flux $q_x\propto e j_x$ (third-order moment), x component of the flux of energy square $\eta_x\propto e q_x$ (fifth-order moment), y component of heat flux $q_y\propto e j_y$ (third-order moment), and y component of the flux of energy square $\eta_y\propto e q_y$ (fifth-order moment). Note that the row vectors are not arranged according to the ascending order of the corresponding moments, but the ordering plays absolutely no role in the analysis.

The equilibria of the nonconserved moments, up to second order in j, are given by [45,53]

$$m_4^{(eq)}=e^{(eq)}=\alpha_2\rho+\beta_2 j\cdot j, \tag{3a}$$

$$m_5^{(eq)}=p_{xx}^{(eq)}=j_x^2-j_y^2, \tag{3b}$$

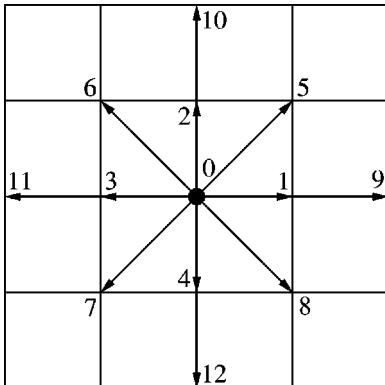
FIG. 1. Discrete velocities of the D2Q13S model. The first nine velocities are identical to those for the D2Q9S model.

$$m_6^{(eq)}=p_{xy}^{(eq)}=j_x j_y, \tag{3c}$$

$$m_7^{(eq)}=\varepsilon^{(eq)}=\alpha_3\rho, \tag{3d}$$

$$m_8^{(eq)}=h^{(eq)}=\alpha_4\rho, \tag{3e}$$

$$m_9^{(eq)}=\pi_{xx}^{(eq)}=0, \tag{3f}$$

$$m_{10,12}^{(eq)}=q_{x,y}^{(eq)}=c_1 j_{x,y}, \tag{3g}$$

$$m_{11,13}^{(eq)}=\eta_{x,y}^{(eq)}=c_2 j_{x,y}. \tag{3h}$$

Among the adjustable parameters in equilibria, α_2, β_2, and c_1 are the most important ones. It should be noted that the above equilibria do not include nonlinear terms in terms of momentum j and heat flux q that are not essential for acoustic and hydrodynamic behavior of the system. However, these nonlinear terms can help to improve Galilean invariance of the system by reducing the flow velocity dependence of the viscosity [54].

The first-order (in k) solution of the dispersion equation (cf. Appendix B) gives the sound speed

$$c_s^2=\frac{1}{26}(\alpha_2+28). \tag{4}$$

The Galilean invariance constraint requires that

$$\beta_2=13. \tag{5}$$

The second-order solution of the dispersion equation yields the attenuation rates of the hydrodynamic modes. Isotropy of a model is optimized by setting the prefactors in angular dependent terms in attenuation rates to zero. These terms depend on the adjustable parameters in the model, hence constraints on these parameters can be obtained. In particular, the isotropy of the transverse mode of the linearized collision operator (cf. Appendix B) requires that

TABLE I. The sound speed c_s, the proportional factor A between relaxation rates s_{xx} and s_{xy} as defined in Eq. (7), and the value of parameter c_1, c_1^*, such that $A(c_1^*) = 1$, for 2D athermal models on square lattice.

Model	$c_s^2 > 0$	$A > 0$	c_1^*
D2Q9S	$\dfrac{1}{6}(4 + \alpha_2)$	$\dfrac{(1 - c_1)}{2(2 + c_1)}$	-1
D2Q13S	$\dfrac{1}{26}(28 + \alpha_2)$	$\dfrac{(85 + 49c_1)}{2(10 - 7c_1)}$	$-\dfrac{65}{63}$
D2Q17S	$\dfrac{1}{34}(60 + \alpha_2)$	$\dfrac{(527 - 47c_1)}{2(1054 + 101c_1)}$	$-\dfrac{527}{83}$
D2Q21S	$\dfrac{1}{14}(32 + \alpha_2)$	$\dfrac{(48755 + 697c_1)}{2(16915 + 149c_1)}$	$-\dfrac{4975}{133}$
D2Q25S	$\dfrac{1}{50}(168 + \alpha_2)$	$\dfrac{(3752 - 131c_1)}{(15008 + 667c_1)}$	$-\dfrac{268}{19}$
D2Q29S	$\dfrac{1}{2}(8 + \alpha_2)$	$\dfrac{(352230 + 407c_1)}{(390040 + 1583c_1)}$	$-\dfrac{18905}{588}$
D2Q33S	$\dfrac{1}{22}(120 + \alpha_2)$	$\dfrac{(13570 - 259c_1)}{(54280 + 1409c_1)}$	$-\dfrac{6785}{278}$

$$\left(\frac{1}{s_6} - \frac{1}{2}\right) = \frac{(85 + 49c_1)}{2(10 - 7c_1)}\left(\frac{1}{s_5} - \frac{1}{2}\right), \tag{6a}$$

$$c_2 = 0. \tag{6b}$$

Therefore, $s_6 = s_5$ when $c_1 = -65/63$. In general, the isotropy constraint for the transverse mode always leads to a relationship between s_{xx} and s_{xy} (respectively, the relaxation rates for stresses p_{xx} and p_{xy}),

$$\left(\frac{1}{s_{xy}} - \frac{1}{2}\right) = A\left(\frac{1}{s_{xx}} - \frac{1}{2}\right), \tag{7}$$

where A depends on adjustable parameters (such as c_1) in the equilibria. Note that the isotropy of the shear viscosity leads to the relationship between s_{xx} and s_{xy} such that in general $s_{xx} \neq s_{xy}$. This constraint cannot be recovered from the simple BGK approximation in which $s_i = 1/\tau$.

With the equilibria of the nonconserved moments given by Eq. (3), the transport coefficients of the D2Q13S model are

$$\nu = \frac{1}{70}(85 + 49c_1)\left(\frac{1}{s_5} - \frac{1}{2}\right), \tag{8a}$$

$$\zeta = \frac{1}{26}(11 + 13c_1 - \alpha_2)\left(\frac{1}{s_4} - \frac{1}{2}\right). \tag{8b}$$

In particular, when $c_1 = c_1^* = -65/63$ (i.e., $s_6 = s_5$),

$$\nu = \frac{31}{63}\left(\frac{1}{s_5} - \frac{1}{2}\right), \tag{9a}$$

$$\zeta = \left(\frac{62}{63} - c_s^2\right)\left(\frac{1}{s_4} - \frac{1}{2}\right). \tag{9b}$$

The positivity of the bulk viscosity ζ gives the upper bound for the sound speed:

$$c_s^2 < \frac{1}{2}(3 + c_1), \tag{10}$$

where Eq. (4) has been substituted. In particular, when $c_1 = -65/63$ (i.e., when $s_6 = s_5$), the upper bound of the sound speed is $c_s^2 < 62/63$.

It should be noted that the sound speed in athermal LBE model is a free parameter and that Eq. (3a) can be rewritten as

$$m_4^{(\mathrm{eq})} = 2(13c_s^2 - 14)\rho + 13\mathbf{j} \cdot \mathbf{j}. \tag{11}$$

In practice, the numerical value of sound speed is determined by the linear stability analysis [45]. Specifically, the linearly optimal value of the sound speed can be obtained numerically by minimizing the dependence of the eigenvalues of the dispersion equation in $\mathbf{k}$ space with respect to a mean flow velocity. We also note that other parameters [α_3 and α_4 in Eqs. (3)] in the equilibria of nonconserved moments $\{m_i^{(\mathrm{eq})} | i = (D+2), \ldots, (b+1)\}$ have little effect on the large scale hydrodynamic (small wave number k) behavior of the system, they do, however, play a role at small scales (large wave number k). In particular, they affect the numerical stability of the model. Therefore, their values should be carefully chosen via linear stability analysis, similar to the way the value of c_s (or equivalently α_2) is determined [45].

For various 2D athermal LBE models, we provide in Table I the sound speed c_s as a function of the parameter α_2, the proportionality factor A between s_{xx} and s_{xy} [as defined in Eq. (7)], and the value c_1^* of c_1, such that $A(c_1^*) = 1$, and hence $s_{xy} = s_{xx}$. Table I includes models up to 33 velocities. These models only include the velocities along axial and

TABLE II. β_2, A_ν, and A_ζ in 2D athermal models on square lattice.

Model	β_2	$A_\nu > 0$	$A_\zeta > 0$
D2Q9S	3	$\frac{1}{6}(1-c_1)$	$\frac{1}{6}(1+c_1-\alpha_2)=\frac{1}{6}(5+c_1-6c_s^2)$
D2Q13S	13	$\frac{1}{70}(85+49c_1)$	$\frac{1}{26}(11+13c_1-\alpha_2)=\frac{1}{2}(3+c_1-2c_s^2)$
D2Q17S	17	$\frac{1}{930}(527-47c_1)$	$\frac{1}{102}(109+17c_1-3\alpha_2)=\frac{1}{6}(17+c_1-6c_s^2)$
D2Q21S	7	$\frac{1}{23880}(48755+697c_1)$	$\frac{1}{168}(197+7c_1-12\alpha_2)=\frac{1}{24}(83+c_1-24c_s^2)$
D2Q25S	25	$\frac{1}{3216}(3752-131c_1)$	$\frac{1}{150}(371+25c_1-3\alpha_2)=\frac{1}{6}(35+c_1-6c_s^2)$
D2Q29S	1	$\frac{1}{115420}(352230+407c_1)$	$\frac{1}{58}(141+c_1-29\alpha_2)=\frac{1}{58}(373+c_1-116c_s^2)$
D2Q33S	11	$\frac{1}{6900}(13570-259c_1)$	$\frac{1}{66}(289+11c_1-3\alpha_2)=\frac{1}{6}(59+c_1-6c_s^2)$

diagonal directions. However, our analysis also shows that the results remain qualitatively the same when velocity sets other than along the axial and diagonal directions, such as $(\pm 1, \pm 2)$ and $(\pm 2, \pm 1)$, are considered. For instance, increasing the number of velocity cannot change the dependence of c_s on α_2, as given by Eq. (4), but the numerical constants in Eq. (4) depend on the velocity set. As the number of velocities and the maximum (particle) speed increase, so does the upper bound of the sound speed, and hence the valid range of α_2 within which $c_s > 0$ widens. The similar observation can be made on parameter c_1. These observations are summarized in Table I.

In general, we can write the viscosities as the following:

$$\nu = A_\nu \left(\frac{1}{s_{xx}} - \frac{1}{2} \right), \tag{12a}$$

$$\zeta = A_\zeta \left(\frac{1}{s_e} - \frac{1}{2} \right), \tag{12b}$$

where s_{xx} and s_e are the relaxation rates for $p_{xx} \propto (j_x^2 - j_y^2)$ and $e \propto \boldsymbol{j} \cdot \boldsymbol{j}$, respectively. Table II provides the value of the parameter β_2 in $m_4^{(eq)} = e^{(eq)}$ [cf. Eq. (3a)], A_ν and A_ζ for the 2D athermal models in Table I. The important observation to note here is that once the collision and advection rules are chosen, the large scale hydrodynamic properties of the LBE model does not change as the number of discrete velocities increases.

III. ENERGY-CONSERVING LBE MODELS

In order to simulate thermohydrodynamics, the energy conservation must be satisfied. Therefore, in addition to the mass density and momentum, there is one more slowly evolving mode that is related to the temperature of real fluids. The energy conservation immediately makes the parameters α_2 and β_2 become fixed constants [cf. Eq. (3a)], consequently the sound speed c_s [which depends on α_2 for athermal models, cf. Eq. (4)] cannot be adjusted by the same parameter(s) in the equilibria of the moments as in the athermal models, but it depends on other parameter(s) in the equilibria. As will be shown below, the kinetic equivalence of the isothermal sound speed depends only on the discrete velocity set for the model, that is, once the velocity set is given, the isothermal sound speed is a fixed constant, unless additional degrees of freedom reminiscent of the internal energy in mo-

lecular gases is introduced. However, the equivalent adiabatic sound speed c_s can be tuned with some parameters in the model (other than α_2 and β_2), and thus one can define an equivalent ratio of specific heats $\gamma = C_P / C_V$.

A. The acoustic properties

The equilibria of the nonconserved moments for the energy conserving LBE models differ from their athermal counterparts. Besides, the energy-mode $|m_4\rangle$ becomes a conserved mode, the equilibrium of the mode $|m_7\rangle = |\varepsilon\rangle$ has to be redefined. For the energy-conserving D2Q13S model,

$$m_7^{(eq)} = \varepsilon^{(eq)} = \alpha_3 \rho + \beta_3 e. \tag{13}$$

Moreover, in order to achieve Galilean invariance for the sound and energy modes, we have to include nonlinear contributions to the equilibria of nonconserved moments. In particular, we have

$$\boldsymbol{q}^{(eq)} = (c_1 + h_1 \rho + k_1 e) \boldsymbol{j}, \tag{14}$$

where $\boldsymbol{q} = (q_x, q_y) = (m_{10}, m_{12})$ corresponds to the heat flux, and $\boldsymbol{j} = (j_x, j_y) = (m_2, m_3)$ is the momentum. The equilibria of nonconserved moments other than $m_8 = h \propto e^3$, $m_{10} = q_x$, and $m_{12} = q_y$ remain the same as in Eq. (3). It turns out that the parameter α_3 in $m_7^{(eq)}$ is proportional to c_1. Specifically, for the energy-conserving D2Q13S model, we have the following results obtained via the linear analysis:

$$\alpha_3 = \frac{1078}{13} c_1, \tag{15a}$$

$$h_1 = \frac{17}{13} - c_1, \tag{15b}$$

$$k_1 = \frac{2}{13}. \tag{15c}$$

With the equilibria given above, the sound speed of the model is

$$c_s = \sqrt{\gamma} c_{s0}, \tag{16a}$$

$$c_{s0} = \sqrt{14/13}, \tag{16b}$$

$$\gamma = \frac{13}{28}(3 + c_1). \tag{16c}$$

The quantity c_{s0} is the isothermal sound speed of the model, and γ is the ratio of specific heats ($=C_P/C_V$), and thus c_s is the adiabatic sound speed. It should be stressed that the isothermal (athermal) sound speed c_{s0} does not depend on the adjustable parameters in the model:

$$c_{s0}^2 = \frac{dp_0}{d\rho} = \frac{e_K}{\rho} = \frac{1}{2B}\sum_i \boldsymbol{c}_i \cdot \boldsymbol{c}_i, \tag{17}$$

where B is the total number of the discrete velocities (including the zero velocity), and p_0 and e_K are the static pressure and the specific kinetic energy. Equation (17) for c_{s0} is identical to the results for c_s in Table I with $\alpha_2 = 0$. Obviously the isothermal sound speed c_{s0} is fixed once the velocity set is chosen. Changing the relative populations of particles with different speeds (in order to mimic the effect of the temperature of Maxwell's distribution in a real gas) has no effect on sound, which is a dynamic effect. One would probably need to use more complicated relaxation equations for the moments to be able to modify the speed of sound. Note, however, that one could add some internal degrees of freedom to allow changes in the speed of sound, as exists in molecular gases. A simple LGA model was studied along this direction [55].

The immediate ramification of Eq. (17) is that, with the polynomial equilibria and relaxation-type collision operators, the sound speed c_s in the energy-conserving LBE model cannot have the correct temperature dependence. It is not clear how to construct nonpolynomial equilibria while still insisting on Galilean invariance within the LBE framework assumed here. This is an intrinsic defect in the energy-conserving LBE models with (linear) relaxational collision. We note that the models on the triangular lattice seem to have a temperature-dependent sound speed [16,56]. This is due to the fact that with the triangular lattice, the condition $s_{xx} = s_{xy}$ alone guarantees the isotropy (of the viscosity) independent of the parameter c_1. The sound speed in these models [16,56] is $c_s^2 = \gamma(c_1)c_{s0}^2$, where $\gamma(c_1)$ is a linear function of c_1. Effectively, the degree of freedom rendered by the parameter c_1 is used to mimic the temperature effect by directly relating c_1 to e (or T). Nevertheless, the isothermal sound speed c_{s0} remains independent of the temperature in these models.

The isotropy of the shear mode and that of the heat flux require, respectively, that

$$\left(\frac{1}{s_6} - \frac{1}{2}\right) = \frac{(85 + 49c_1)}{2(10 - 7c_1)}\left(\frac{1}{s_5} - \frac{1}{2}\right), \tag{18a}$$

$$s_{12} = s_{10}. \tag{18b}$$

The coupling between s_5 and s_6 is identical to that for the athermal D2Q13S model [cf. Eq. (6a)]. Note that the sound speed c_s is a function of c_1 (the parameter in $\boldsymbol{q}^{(eq)} = c_1\boldsymbol{j}$) for the energy-conserving model, as opposed to a function of α_2 for the athermal model [cf. Eq. (4) and Table I]. Thus the

parameter c_1 affects both the sound speed c_s and the relaxation rate s_6 simultaneously for energy-conserving models. In other words, for the athermal models, the coupling between "energy" mode e (which is not a conserved quantity) and density mode ρ controls the acoustics, whereas in the energy-conserving models, it is the coupling between the heat flux $\boldsymbol{q}$ and the momentum $\boldsymbol{j}$ that renders the same effect.

B. Transport coefficients

With the energy conservation, the model now has four hydrodynamic modes: two relax (energy and shear modes) and two propagate (sound). In the large scale limit, the attenuation rates of these modes are proportional to k^2 and are given below,

$$\gamma_\perp = \nu k^2, \tag{19a}$$

$$\gamma_\pm = \frac{1}{2}\left(\nu + \frac{(\gamma - 1)}{\gamma}\kappa\right)k^2, \tag{19b}$$

$$\gamma_T = \frac{\kappa}{\gamma}k^2, \tag{19c}$$

where the transport coefficients of the energy-conserving D2Q13S model are

$$\nu = \frac{(85 + 49c_1)}{70}\left(\frac{1}{s_5} - \frac{1}{2}\right), \tag{20a}$$

$$\kappa = \frac{2(130 + 26\beta_3 - 77c_1)}{143(3 + c_1)}\left(\frac{1}{s_{10}} - \frac{1}{2}\right). \tag{20b}$$

As expected from what is known in real gases, the thermal diffusivity of the model, κ [$=\lambda/(\rho C_V)$], is determined by the relaxation rates $s_{10} = s_{12}$ for the nonconserved moments corresponding to the heat flux [$\boldsymbol{q} = (q_x, q_y)$], and is also related to the coupling parameters c_1 and β_3 in the equilibrium of the fourth-order moment $m_7 = \varepsilon \propto e^2$ [cf. Eq. (13)]. The above formulas thus recover the results for a real gas. One can, in principle, adjust the parameters c_1 and β_3. It should also be noted that in the energy-conserving D2Q13S model, there is no bulk viscosity.

In addition to the D2Q13S model, we also study a number of energy-conserving models with more discrete velocities in two dimensions. Our results are summarized in Tables III–V. Table III provides the parameter values for α_3, h_1, and k_1. Table IV gives the results for the sound speed c_s, the ratio of specific heats γ, and the proportionality factor A relating relaxation rates s_{xx} and s_{xy}, as defined in Eq. (7). Table V shows the viscosity ν and the thermal diffusivity κ in terms of A_ν and A_κ, where A_ν is defined in Eq. (12a) and A_κ is similarly defined as the following:

$$\kappa = A_\kappa\left(\frac{1}{s_q} - \frac{1}{2}\right), \tag{21}$$

where s_q denotes the relaxation rate for the heat flux $\boldsymbol{q}$. Finally, we observe that in addition to its effect on the thermal

TABLE III. Coefficients for Galilean invariance for 2D TLBE models on square lattice.

Model	α_3	h_1	k_1
D2Q13S	$\dfrac{1078}{13}c_1$	$\dfrac{17}{13}-c_1$	$\dfrac{2}{13}$
D2Q17S	$\dfrac{1090}{17}c_1$	$\dfrac{71}{17}-c_1$	$\dfrac{6}{17}$
D2Q21S	$\dfrac{788}{7}c_1$	$\dfrac{187}{7}-c_1$	$\dfrac{24}{7}$
D2Q25S	$\dfrac{72716}{25}c_1$	$\dfrac{133}{25}-c_1$	$\dfrac{6}{25}$
D2Q29S	$188c_1$	$91-c_1$	58
D2Q33S	$\dfrac{5780}{11}c_1$	$\dfrac{71}{11}-c_1$	$\dfrac{6}{11}$

diffusivity κ, as seen in Eq. (20b) and Table V, parameter β_3 produces no other observable effects. Therefore, for all practical purposes β_3 can be set to zero.

C. Spurious mode coupling and numerical instability

As previously indicated, the analysis of the linearized dispersion equation (B1) yields the constraints on the adjustable parameters in the equilibria of nonconserved moments (α_3, β_3, h_1, and k_1) as well as the relationships between the relaxation rates. The eigenvalues of the linearized evolution operator gives the k dependence of the transport coefficients $\nu(k)$ [$\zeta(k)$] and $\kappa(k)$, and the sound speed $c_s(k)$. Such analysis usually sheds light on the stability of the model under consideration. As an example, we numerically analyze the energy-conserving D2Q13S model with the following parameter values: $c_1 = -0.415\,38$, $\beta_3 = 0$, $s_5 = 1.957\,61$, and

$s_{10} = 1.937\,73$. Henceforth we have $\gamma = 1.2$, the shear viscosity $\nu = 0.01$, the thermal diffusivity $\kappa = 0.016$, and Prandtl number $\mathrm{Pr} = 0.71$ ($\mathrm{Pr} = \gamma\nu/\kappa$). We choose k along two directions: $\theta = 0$ and $\theta = \pi/8$ (22.5°), θ being the polar angle of k (with respect to x axis). Figure 2 shows $\gamma_\perp(k)/\nu$, $\gamma_\pm(k)/\nu$, and $\gamma_h(k)/\nu$, where ν is given by Eq. (20a). For the case of $\theta = \pi/8$ (22.5°), $\gamma_\perp(k)$ and $\gamma_h(k)$ coalesce at about $k = k_c \approx 0.048$, which is a branch point. There is another branch point at about $(\pi - k_c)$, due to the symmetry of the operator L. The critical value k_c at which the first branch point locates is approximately proportional to $\nu\sqrt{|1 - \mathrm{Pr}^{-1}|}$. Between the two branch points $[k_c, \pi - k_c]$, the corresponding eigenvalues $z_\perp(k)$ and $z_T(k)$ coalesce and become complex conjugate to each other, and the corresponding modes become oscillatory. This coupling between the energy and shear modes takes place at a very small value of wave number at $k = k_c$, and continues to a point near $k = \pi - k_c$. It is interesting to note that the spurious coupling between the energy and shear modes is *mathematically* similar to that in the Rayleigh-Bénard convection with a gravity

$$g = \frac{\alpha}{\nu}\sin(4\theta), \tag{22}$$

where α is a complicated algebraic function of γ, κ, ν, and relaxation rates s_e and s_ε, and depends strongly on γ and weakly on other parameters, and θ is the polar angle of k. We find that the energy-conserving LBE models are prone to numerical instabilities which may be instigated by fluctuations of wide-ranged scales. Obviously, this undesirable coupling among the hydrodynamic modes is due to the small number of degrees of freedom and simple spatial-temporal dynamics of the lattice Boltzmann equation. In contrast, the coupling among the modes in the athermal models occurs only at a point near $k = \pi$ (cf. Fig. 1 in Ref. [45]). The athermal models are much more stable and are only prone to

TABLE IV. The sound speed c_s, the ratio of specific heats γ, and A defined in Eq. (7) for 2D TLBE models on square lattice.

Model	$c_s^2 > 0$	γ	$A > 0$
D2Q13S	$\dfrac{1}{2}(3+c_1)$	$\dfrac{14}{13}c_s^2$	$\dfrac{(49c_s^2 - 31)}{(31 - 14c_s^2)}$
D2Q17S	$\dfrac{1}{6}(17+c_1)$	$\dfrac{17}{30}c_s^2$	$\dfrac{(221 - 47c_s^2)}{(202c_s^2 - 221)}$
D2Q21S	$\dfrac{1}{24}(83+c_1)$	$\dfrac{7}{16}c_s^2$	$\dfrac{(697c_s^2 - 379)}{(298c_s^2 + 379)}$
D2Q25S	$\dfrac{1}{6}(35+c_1)$	$\dfrac{25}{84}c_s^2$	$\dfrac{(2779 - 262c_s^2)}{(1334c_s^2 - 2779)}$
D2Q29S	$\dfrac{1}{58}(373+c_1)$	$\dfrac{1}{4}c_s^2$	$\dfrac{(814c_s^2 + 6911)}{(6911 - 3166c_s^2)}$
D2Q33S	$\dfrac{1}{6}(59+c_1)$	$\dfrac{11}{60}c_s^2$	$\dfrac{(9617 - 518c_s^2)}{(2818c_s^2 - 9617)}$

TABLE V. Transport coefficients for 2D TLBE models on square lattice.

Model	$A_\nu > 0$	$A_\kappa > 0$
D2Q13S	$\dfrac{1}{70}(85 + 49c_1)$	$\dfrac{1}{154}(130 + 26\beta_3 - 77c_1)$
D2Q17S	$\dfrac{1}{930}(527 - 47c_1)$	$\dfrac{1}{654}(1054 + 102\beta_3 - 109c_1)$
D2Q21S	$\dfrac{1}{23880}(48755 + 697c_1)$	$\dfrac{1}{4728}(6965 + 56\beta_3 - 197c_1)$
D2Q25S	$\dfrac{1}{3216}(3752 - 131c_1)$	$\dfrac{1}{15582}(53600 + 150\beta_3 - 2597c_1)$
D2Q29S	$\dfrac{1}{115420}(352230 + 407c_1)$	$\dfrac{1}{2726}(7960 + 2\beta_3 - 47c_1)$
D2Q33S	$\dfrac{1}{6900}(13570 - 259c_1)$	$\dfrac{1}{1734}(10120 + 66\beta_3 - 289c_1)$

instabilities due to small scale fluctuations. It must be stressed that this coupling between the viscous and energy modes is common to all the energy-conserving LBE models that we have studied. The fact that it depends very little on the relaxational properties of higher order moments convince us to believe that it cannot be eliminated by increasing the number of discrete velocities. However, we observe that in-

FIG. 2. Attenuation rates for the hydrodynamic modes of the D2Q13S model. The rates for the viscous and thermal modes that are given by $\gamma_\perp$ and γ_h, are normalized by the shear viscosity ν. The rate for the sound modes $\gamma_\pm$ is normalized by its value at $\boldsymbol{k} = \boldsymbol{0}$, i.e., $\gamma_\pm(0) = [\nu + (\gamma - 1)\kappa/\gamma]/2$, $\gamma = 1.2$, $\nu = 0.01$, and Pr $= \gamma\nu/\kappa = 0.71$. (a) The polar angle of the wave vector $\boldsymbol{k}$, $\theta = 0°$. All the hydrodynamic modes are decoupled and have weak k dependence along this direction. (b) $\theta = 22.5°$. The viscous mode $\gamma_\perp$ and the energy mode γ_h are coupled at about $k = 0.048$ and show strong k-dependent behavior.

terpolations can smear the mode-mode coalescence and this explains, in part, the reason why the TLBE schemes with interpolations [12–14,20,21,27–31] tend to be more stable numerically.

IV. HYBRID TLBE MODELS

As indicated previously, the spurious mode coupling and numerical instability in the energy-conserving LBE models cannot be overcome by increasing the number of discrete velocities or including higher order terms in the equilibria. However, the athermal LBE models do not have such problems. Therefore, we come to the conclusion that at present time the best approach to formulate a TLBE model is to treat the energy-conservation equation separately from the mass and momentum conservation equations. Similar treatment was previously advocated to address the issue of numerical efficiency [33,34]. This means that the lattice Boltzmann equation is used to simulate the mass and momentum conservation laws, and a finite-difference scheme (or other means) is used to solve the diffusion-advection equation for the temperature, with appropriate couplings between the equations.

A. 9-velocity model in two dimensions

We now illustrate the hybrid TLBE model using the D2Q9S model. The moment corresponding to the energy, $m_4 = e$, is not a conserved moment, and its equilibrium is coupled to the temperature T (which is to be simulated by means other than the lattice Boltzmann equation). The coupling between the energy mode $m_4 = e$ and the temperature T is chosen as

$$m_4^{(\mathrm{eq})} = e^{(\mathrm{eq})} = 6\left(c_{s0}^2 - \frac{2}{3}\right)\rho + (2 - \gamma)\boldsymbol{j}\cdot\boldsymbol{j} + 6q_1 T, \quad (23)$$

where q_1 is a coupling coefficient to be determined later. The isothermal sound speed c_{s0} is an adjustable constant determined by the positivity of the bulk viscosity [cf. Eq. (29b)]
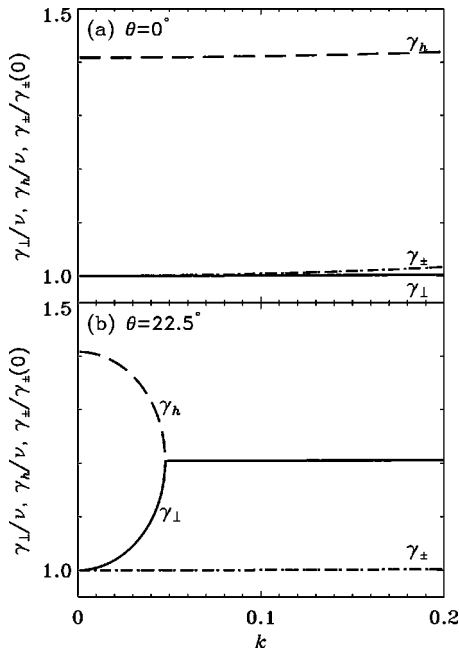
and other stability criteria, and the ratio of specific heats (γ) is an adjustable parameter in the model. The temperature T evolves according to the standard diffusion-advection equation,

$$\partial_t T + \boldsymbol{u} \cdot \boldsymbol{\nabla} T = \kappa \Delta T + q_2(\gamma - 1)c_{s0}^2 \boldsymbol{\nabla} \cdot \boldsymbol{u}, \qquad (24)$$

where κ is the thermal diffusivity as in Eq. (20b) and the coupling coefficient q_2 is to be determined later. It should be noted that the density ρ does not appear in Eq. (24) for the following reason. In general, the lattice Boltzmann equation considers density variations while it intends to solve the nearly incompressible (or weakly compressible) Navier-Stokes equations. Theoretically speaking, the density variations should be so small that they can be neglected except where they play a dominant role (e.g., in acoustics). The nonlinear terms are small corrections in the low Mach number limit, and therefore the density can be treated as a constant in the nonlinear terms. This rationale allows us to use $\rho = \rho_0 = 1$ in the nonlinear terms, and $\delta\rho = (\rho - \rho_0)$ in those terms linear in ρ. This practice helps to reduce the effects of round-off errors in simulations [50,57]. It also permits us to replace the velocity $\boldsymbol{u}$ in Eq. (24) by the momentum $\boldsymbol{j} = (j_x, j_y)$ obtained from the LBE model.

It is important to note that Eq. (24) of T does not have the nonlinear terms related to $(\boldsymbol{\nabla} \cdot \boldsymbol{j})^2$ and $(\partial_i u_j + \partial_j u_i)^2$, as in the energy equation for compressible fluids (e.g., Refs. [58,59]). The reasons we neglect these terms are that we restrict our focus here on the acoustics of the LBE system, which is essentially of linear nature, and these nonlinear terms are, in fact, negligible for incompressible fluids. However, the framework set used here does allow us to include these nonlinear terms, which are to be considered in our future work.

The advection-convection equation (24) for the temperature T is solved by the following finite-difference equation:

$$T(\boldsymbol{r}_j, t+1) - T(\boldsymbol{r}_j, t) = -\boldsymbol{j} \cdot \boldsymbol{\nabla}^* T + \kappa \Delta^* T$$
$$+ q_2(\gamma - 1)c_{s0}^2 \boldsymbol{\nabla}^* \cdot \boldsymbol{j}, \qquad (25)$$

where operators with superscript $*$ are the corresponding finite-difference operators [cf. Appendix C]. The stencil used for the finite-difference operators must have the same symmetries as those of the discrete velocity set of the model, i.e., it is a nine-point stencil for the D2Q9S model. It should be emphasized that the use of the stencil defined by the discrete velocity set does help to improve the numerical stability of the scheme. In contrast, the use of the simple five-point central difference stencil, in fact, leads to severe numerical instability. We should also point out that the stencils which have the same symmetries of the discrete velocity set are not unique, although the lattice Boltzmann equation uniquely defines a specific set of weighted stencils [60,61]. We have not studied the influence due to the different stencils on the stability and the nonhydrodynamic behavior (in $\boldsymbol{k}^4$ or higher order) of the model.

In the setting of the HTLBE method, there are $(9+1)$ degrees of freedom at each lattice site. The linear analysis of the dispersion equation gives the sound speed of the model as

$$c_s^2 = [1 + (\gamma - 1)q_1 q_2]c_{s0}^2. \qquad (26)$$

In order to have $c_s^2 = \gamma c_{s0}^2$ as in the real monoatomic gases, and a correct coupling between the momentum $\boldsymbol{j}$ and the temperature T [in Eq. (30)], we must have

$$q_1 = q_2 = 1. \qquad (27)$$

Note that the sound speed of Eq. (26) is independent of the temperature in this model, indicating an inherent deficiency of the lattice Boltzmann equation.

There are four hydrodynamic modes in the system: one transverse mode (shear mode) and three longitudinal modes (two acoustic modes and one energy mode). Again, the isotropy of the transverse mode demands that the relaxation rates s_5 and s_6, corresponding, respectively, to the diagonal and off-diagonal components of the stress tensor, must satisfy a relationship similar to Eq. (7) with the coefficient A given in Table I. The attenuation coefficients for the four hydrodynamic modes are similar to those in Eqs. (19), except $\gamma_\pm$ for the acoustic modes. The previous analysis needs to be slightly modified to include the discrete effects due to the finite-difference equation (25) for T. This leads to a correction for the attenuation rate of sound waves as the following:

$$\gamma_\pm = \frac{1}{2}\left[\nu + \zeta + \frac{(\gamma - 1)}{\gamma}\left(\kappa - \frac{1}{2}\gamma c_{s0}^2 \right) \right]. \qquad (28)$$

The correction $\gamma c_{s0}^2/2$ is similar to the "propagation" contribution to the viscosity first found by Hénon in the context of the lattice gases automata [62]. The transport coefficients ν and ζ in this model are identical to the previous results for athermal models given in Eq. (12) and Table II. Specifically, with $c_1 = -1$ and thus $s_6 = s_5$, the viscosities of the model are

$$\nu = \frac{1}{3}\left(\frac{1}{s_6} - \frac{1}{2} \right), \qquad (29a)$$

$$\zeta = \left(\frac{2}{3} - \gamma c_{s0}^2 \right)\left(\frac{1}{s_4} - \frac{1}{2} \right). \qquad (29b)$$

The Chapman-Enskog analysis for the system consisting of the lattice Boltzmann equation (1) and the finite-difference equation (25) for T leads to the following set of hydrodynamic equations:

$$\partial_t \rho + \boldsymbol{\nabla} \cdot \boldsymbol{j} = 0, \qquad (30a)$$

$$\partial_t \boldsymbol{j} + \boldsymbol{j} \cdot \boldsymbol{\nabla} \boldsymbol{j} = -c_{s0}^2 \boldsymbol{\nabla} \rho + \nu \Delta \boldsymbol{j} + \zeta \boldsymbol{\nabla}\boldsymbol{\nabla} \cdot \boldsymbol{j} + q_1 \boldsymbol{\nabla} T, \quad (30b)$$

$$\partial_t T + \gamma \boldsymbol{j} \cdot \boldsymbol{\nabla} T = \kappa \Delta T + q_2(\gamma - 1)c_{s0}^2 \boldsymbol{\nabla} \cdot \boldsymbol{j}, \qquad (30c)$$

where $q_1 = q_2 = 1$. Because the constant γ appears in the advection term in Eq. (30c), this equation must be rescaled.

Effectively, this reduces κ by a factor γ, i.e., $\kappa_{\text{eff}} = \kappa/\gamma$. In the HTLBE scheme, κ is an independent parameter.

The results for the transport coefficients of the HTLBE model are similar to that of the athermal LBE model. That is, the isothermal sound speed c_{s0} is an adjustable parameter in the model and there is also a nonzero bulk viscosity ζ. The linear stability analysis shows that, so long as γ is not too far away from 1, the HTLBE model is as stable as the athermal model, i.e., the finite-difference equation for T does not have much effect on the stability of the model, provided that the appropriate finite-difference stencils are used. Further analysis shows that there is no spurious coupling between the energy and shear modes that exists in the energy-conserving models, as shown in Fig. 2. It should be pointed out that the present approach of hybrid schemes can be easily and effectively extended to other situations. In particular, a second scalar equation solved by finite-difference technique can be added to simulate double diffusions.

B. Models in three dimensions

1. 13-velocity model

We now proceed to consider the HTLBE models in three dimensions. For the LBE part we use the simplest model with just 13 velocities (D3Q13) [49]. The transformation matrix M of the model is given in Appendix D. The equilibria of the nonconserved moments are chosen as follows:

$$m_5^{(\text{eq})} = e^{(\text{eq})} = \frac{39}{2}\left(c_{s0}^2 - \frac{8}{13}\right)\rho + \frac{39}{4}\left(\frac{5}{3} - \gamma\right)\boldsymbol{j}\cdot\boldsymbol{j} + \frac{39}{2}q_1 T,$$

$$(31a)$$

$$m_6^{(\text{eq})} = 3p_{xx}^{(\text{eq})} = 2j_x^2 - j_y^2 - j_z^2 = 3j_x^2 - \boldsymbol{j}\cdot\boldsymbol{j}, \quad (31b)$$

$$m_7^{(\text{eq})} = p_{ww}^{(\text{eq})} = j_y^2 - j_z^2, \quad (31c)$$

$$m_8^{(\text{eq})} = p_{xy}^{(\text{eq})} = j_x j_y, \quad (31d)$$

$$m_9^{(\text{eq})} = p_{yz}^{(\text{eq})} = j_y j_z, \quad (31e)$$

$$m_{10}^{(\text{eq})} = p_{zx}^{(\text{eq})} = j_z j_x, \quad (31f)$$

$$m_{11,12,13}^{(\text{eq})} = \varphi_{x,y,z}^{(\text{eq})} = 0. \quad (31g)$$

And temperature T is solved by the scheme given by Eq. (25), with the stencil defined by the 13-velocity set (cf. Appendix D).

There are five hydrodynamic modes in the model: two transverse modes and three longitudinal ones. Among the three longitudinal modes, two acoustic modes propagate with the adiabatic speed of sound $c_s = \sqrt{\gamma} c_{s0}$, and one energy mode relaxes (or diffuses). The isotropy constraints on the attenuation rates lead to

$$s_7 = s_6, \quad (32a)$$

$$\left(\frac{1}{s_8} - \frac{1}{2}\right) = \frac{1}{2}\left(\frac{1}{s_6} - \frac{1}{2}\right), \quad (32b)$$

$$s_{10} = s_9 = s_8. \quad (32c)$$

The isotropy of the model is evident because the attenuation rates (proportional to k^2) for these modes are independent of the direction of $\boldsymbol{k}$:

$$\gamma_\perp = \nu k^2, \quad (33a)$$

$$\gamma_h = \frac{\kappa}{\gamma} k^2, \quad (33b)$$

$$\gamma_\pm = \frac{1}{2}\left[\frac{4}{3}\nu + \zeta + \frac{(\gamma-1)}{\gamma}\left(\kappa - \frac{1}{2}\gamma c_{s0}^2\right)\right]k^2, \quad (33c)$$

as expected for a real gas. Note that the above formula for $\gamma_\pm$ includes the correction due to the second-order discrete effect (Hénon correction), similar to the 2D result of Eq. (28). The transport coefficients ν and ζ in this model are given by Eq. (12) and Table II. Specifically, with $c_1 = 0$,

$$\nu = \frac{1}{2}\left(\frac{1}{s_6} - \frac{1}{2}\right), \quad (34a)$$

$$\zeta = \left(\frac{2}{3} - \gamma c_{s0}^2\right)\left(\frac{1}{s_5} - \frac{1}{2}\right). \quad (34b)$$

The Chapman-Enskog analysis for the HTLBE system is that the conserved moments [ρ and $\boldsymbol{j} \equiv (j_x, j_y, j_z)$] and T evolve according to the following equations, similar to Eqs. (30) in two dimensions:

$$\partial_t \rho + \boldsymbol{\nabla} \cdot \boldsymbol{j} = 0 \quad (35a)$$

$$\partial_t \boldsymbol{j} + \boldsymbol{j} \cdot \boldsymbol{\nabla} \boldsymbol{j} = -c_{s0}^2 \boldsymbol{\nabla} \rho + \nu \Delta \boldsymbol{j} + \left(\frac{1}{3}\nu + \zeta\right)\boldsymbol{\nabla} \boldsymbol{\nabla} \cdot \boldsymbol{j} + q_1 \boldsymbol{\nabla} T,$$

$$(35b)$$

$$\partial_t T + \gamma \boldsymbol{j} \cdot \boldsymbol{\nabla} T = \kappa \Delta T + q_2 (\gamma-1) c_{s0}^2 \boldsymbol{\nabla} \cdot \boldsymbol{j}. \quad (35c)$$

Again, we must set $q_1 = q_2 = 1$ in order to have $c_s^2 = \gamma c_{s0}^2$, as before.

The linear stability analysis shows that it is necessary to use the stencils that have the same symmetries of the discrete velocity set in the finite-difference equation (25) for T. Using a simpler seven-point central difference stencil would generate severe numerical instability. With the stencil generated from the discrete velocity set, the stability of the hybrid TLBE system is almost the same as the stability of the lattice Boltzmann equation alone. That is, the finite-difference equation for T with appropriate stencils has little effect on the stability. Because the stencil generated by the discrete velocity set naturally preserves the parity of the model, $\chi = (i+j+k)(\text{mod }2)$ at a site (i,j,k), which is conserved in the model [49], one can save one-half of the system size in simu-

lations by considering only the sites with even or odd parity [49]. This is a unique feature of the 13-velocity model in three dimensions.

2. 15-velocity model

The 15-velocity model in three-dimensional cubic lattices has three particle speeds: 0, 1, and $\sqrt{3}$. The corresponding moments are arranged in the following order:

$$(\rho, e, \epsilon, j_x, q_x, j_y, q_y, j_z, q_z, 3p_{xx}, p_{ww}, p_{xy}, p_{yz}, p_{zx}, \psi_{xyz}),$$

and the transformation matrix M with the corresponding order of the row vectors is given in Appendix E.

The equilibria are given by

$$m_2^{(eq)} = e^{(eq)} = 3\left(c_{s0}^2 - \frac{2}{3}\right)\rho + \frac{3}{2}\left(\frac{5}{3} - \gamma\right)\mathbf{j} \cdot \mathbf{j} + 3T, \tag{36a}$$

$$m_3^{(eq)} = \varepsilon^{(eq)} = \alpha_3 \rho, \tag{36b}$$

$$m_{5,7,9}^{(eq)} = q_{x,y,z}^{(eq)} = c_1 j_{x,y,z}, \tag{36c}$$

$$m_{15}^{(eq)} = \psi_{xyz}^{(eq)} = 0, \tag{36d}$$

where $\alpha_3 = -1$ is a constant that plays no role in hydrodynamics. The equilibria of $(3p_{xx}, p_{ww}, p_{xy}, p_{yz}, p_{zx}) = (m_{10}, m_{11}, m_{12}, m_{13}, m_{14})$ are identical to that in Eq. (31).

The relaxation rates $\{s_i | i = 1, 2, \ldots, 15\}$ satisfy the following constraints due to isotropy criteria:

$$s_{11} = s_{10} \quad \text{for } p_{ww} \text{ and } p_{xx}, \tag{37a}$$

$$s_{14} = s_{13} = s_{12} \quad \text{for } p_{zx}, \ p_{yz}, \text{ and } p_{xy}, \tag{37b}$$

$$\left(\frac{1}{s_{12}} - \frac{1}{2}\right) = \frac{(1 - c_1)}{2(4 + c_1)}\left(\frac{1}{s_{10}} - \frac{1}{2}\right), \tag{37c}$$

$$s_5 = s_7 = s_9 \quad \text{for } \mathbf{q} = (q_x, q_y, q_z). \tag{37d}$$

The transport coefficients of the model are

$$\nu = \frac{(1 - c_1)}{10}\left(\frac{1}{s_{xx}} - \frac{1}{2}\right), \tag{38a}$$

$$\zeta = \frac{(13 + 2c_1 - 15\gamma c_{s0}^2)}{15}\left(\frac{1}{s_e} - \frac{1}{2}\right), \tag{38b}$$

where s_{xx} ($=s_{10}$) and s_e ($=s_2$) denote the relaxation rates for moments p_{xx} and e, respectively.

The temperature T evolves according to the finite-difference equation (25), with the stencils generated by the 15-velocity set (cf. Appendix E). The resulting hydrodynamic equations are given by Eq. (35) with $q_1 = q_2 = 1$.

3. 19-velocity model

The particle speed in the 19-velocity model in three dimensions are 0, 1, and $\sqrt{2}$. The corresponding 19 moments are arranged according to the following order [50]:

$$(\rho, e, \varepsilon, j_x, q_x, j_y, q_y, j_z, q_z, 3p_{xx}, 3\pi_{xx}, p_{ww},$$

$$\pi_{ww}, p_{xy}, p_{yz}, p_{xz}, \varphi_x, \varphi_y, \varphi_z).$$

The transformation matrix M is given in Appendix F.

The equilibrium quantities are given by

$$m_2^{(eq)} = e^{(eq)} = 57\left(c_{s0}^2 - \frac{10}{19}\right)\rho + \frac{57}{2}\left(\frac{5}{3} - \gamma\right)\mathbf{j} \cdot \mathbf{j} + 57T, \tag{39a}$$

$$m_3^{(eq)} = \varepsilon^{(eq)} = \alpha_3 \rho, \tag{39b}$$

$$m_{11} = 3\pi_{xx}^{(eq)} = 0, \quad m_{13} = \pi_{ww}^{(eq)} = 0, \tag{39c}$$

where $\alpha_3 = 3$ is a constant that has no relevant role in hydrodynamics. The equilibria of $(3p_{xx}, p_{ww}, p_{xy}, p_{yz}, p_{zx}) = (m_{10}, m_{12}, m_{14}, m_{15}, m_{16})$ and $(\varphi_x, \varphi_x, \varphi_z) = (m_{17}, m_{18}, m_{19})$ are identical to that in Eq. (31), and the equilibria of $\mathbf{q} = (q_x, q_y, q_z) = (m_5, m_7, m_9)$ are identical to that in Eq. (36).

The relaxation rates $\{s_i | i = 1, 2, \ldots, 19\}$ must satisfy the following constraints for the sake of isotropy:

$$s_{12} = s_{10} \quad \text{for } p_{ww} \text{ and } p_{xx}, \tag{40a}$$

$$s_{16} = s_{15} = s_{14} \quad \text{for } p_{zx}, p_{yz}, \text{ and } p_{xy}, \tag{40b}$$

$$\left(\frac{1}{s_{14}} - \frac{1}{2}\right) = \frac{(6 - c_1)}{2(4 + c_1)}\left(\frac{1}{s_{10}} - \frac{1}{2}\right), \tag{40c}$$

$$s_5 = s_7 = s_9 \quad \text{for } \mathbf{q} = (q_x, q_y, q_z). \tag{40d}$$

The viscosities of the model are

$$\nu = \frac{(6 - c_1)}{20}\left(\frac{1}{s_{xx}} - \frac{1}{2}\right), \tag{41a}$$

$$\zeta = \frac{(9 + c_1 - 15\gamma c_{s0}^2)}{15}\left(\frac{1}{s_e} - \frac{1}{2}\right), \tag{41b}$$

where s_{xx} ($=s_{10}$) and s_e ($=s_2$) denote the relaxation rates for moments p_{xx} and e, respectively.

C. Summary of the hybrid thermal lattice Boltzmann equation

The hybrid thermal lattice Boltzmann model is summarized as follows. The evolution equations for the distribution functions and the temperature are

$$|f(\mathbf{r}_j + \mathbf{c}_i, t_n + 1)\rangle = |f(\mathbf{r}_j, t_n)\rangle - \mathsf{M}^{-1}\mathsf{S}[|m(\mathbf{r}_j, t_n)\rangle - |m^{(eq)}(\mathbf{r}_j, t_n)\rangle], \tag{42a}$$

$$T(\mathbf{r}_j, t + 1) - T(\mathbf{r}_j, t) = -\mathbf{j} \cdot \nabla^* T + \kappa \Delta^* T + q_2(\gamma - 1) \times c_{s0}^2 \nabla^* \cdot \mathbf{j}. \tag{42b}$$

The coupling of the temperature T to the fluid momentum $\mathbf{j}$ is explicit in the above equation for T. The coupling of the fluid momentum $\mathbf{j}$ to the temperature T is accomplished in the

equilibrium of the second-order moment e (related to energy). The equilibria of e and the fourth-order moment ε (related to energy square) are

$$e^{(\text{eq})} = \alpha_2 \rho + \beta_2 \boldsymbol{j} \cdot \boldsymbol{j} + q_1 T, \tag{43a}$$

$$\varepsilon^{(\text{eq})} = \alpha_3 \rho, \tag{43b}$$

where both $\alpha_2 = \alpha_2(c_{s0}^2)$ and $\beta_2 = \beta_2(\gamma)$ are determined by the first-order solution of the linearized dispersion equation. The coefficient α_2 depends on the (isothermal) sound speed c_{s0} that is an adjustable parameter in the model, while the coefficient β_2 affects the Galilean invariance and depends on the adjustable parameter γ. And the value of the parameter α_3 is determined so that in the equation for T the term linear in the density gradient $\nabla \rho$ vanishes. The other two coefficients in the model, q_1 and q_2, are determined by the linear analysis and the Chapman-Enskog analysis so that the hydrodynamic equations derived from the model are

$$\partial_t \rho + \nabla \cdot \boldsymbol{j} = 0, \tag{44a}$$

$$\partial_t \boldsymbol{j} + \boldsymbol{j} \cdot \nabla \boldsymbol{j} = -c_{s0}^2 \nabla \rho + \nu \Delta \boldsymbol{j} + \zeta' \nabla \nabla \cdot \boldsymbol{j} + \nabla T, \tag{44b}$$

$$\partial_t T + \gamma \boldsymbol{j} \cdot \nabla T = \kappa \Delta T + (\gamma - 1) c_{s0}^2 \nabla \cdot \boldsymbol{j}, \tag{44c}$$

where $\zeta' = \zeta$ in two dimensions and $\zeta' = \zeta + \nu/3$ in three dimensions, with the adiabatic sound speed

$$c_s^2 = \gamma c_{s0}^2. \tag{}$$

The viscosities ν and ζ are controlled by the relaxation rates s_{xx} and s_e, respectively, and κ and γ are adjustable parameters in the model.

We note that, because T could be solved by more accurate numerical techniques other than the second-order finite difference of Eq. (42b), the equilibrium of e given by Eq. (43a) would have to be modified in order to consider nonuniformity of T over one cell (spatial derivatives of T).

The lattice Boltzmann equation can include external fields, such as gravity. For a forcing $\boldsymbol{F}$, one can simply add it to the momentum, by $\boldsymbol{j} + \boldsymbol{F}\delta t \rightarrow \boldsymbol{j}$ ($\delta t = 1$). It is understood that, in order to conserve mass up to the second order in the Chapman-Enskog analysis, the net effect of the forcing term is that the resultant momentum is equal to $\boldsymbol{j} + \boldsymbol{F}\delta t/2$ [63,64]. Therefore it is preferable to execute the forcing term in two steps, adding one-half of the forcing before relaxation and one-half after, and to use the momentum added with one-half of the forcing before relaxation (collision) as the measured field for output [65]. This can be concisely illustrated as follows:

Step 1: Advection of $\{f_i\}$,

Step 2: Compute moments $\{m_i\}$ of $\{f_i\}$,

Step 3: $\boldsymbol{j}' = \boldsymbol{j} + \dfrac{1}{2}\, \boldsymbol{F}$,

Step 4: Relaxations of the moments (collision),

Step 5: $\boldsymbol{j}'' = \boldsymbol{j}' + \dfrac{1}{2}\, \boldsymbol{F}$,

Step 6: Compute $\{f_i\}$ from the moments $\{m_i\}$,

where $\boldsymbol{j}'$ is used as the measured field for output.

Several basic tests have been conducted to verify the properties of the hybrid TLBE model. In a system with uniform flow velocity and periodic boundary conditions, transverse modes (shear waves) and longitudinal modes (sound waves and energy mode) are found to have correct attenuation rates and advection/propagation velocity in the long wavelength limit of $\boldsymbol{k} \rightarrow \boldsymbol{0}$, as predicted by the linear analysis. To ensure accurate tests for longitudinal modes, one must use the initial conditions which are prepared to have pure acoustic or thermal character to excite only these modes.

V. SIMULATIONS

We use the 13-velocity HTLBE model in 3D to simulate the Rayleigh-Bénard convective flows in the cubic cavity with two opposite vertical walls at different temperatures. The geometry of the cavity is depicted in Fig. 3. The box size is $N_x \times N_y \times N_z$, where $N_x = N_y = 50$ is fixed throughout the simulations while N_z varies from 6 to 80. For the lattice Boltzmann part, the bounce-back boundary conditions are applied for six walls. As for the temperature, two opposite vertical walls located at $x = 1/2$ and $x = N_x + 1/2 = 50 + 1/2$ (because of the bounce-back boundary conditions) are maintained with constant temperatures $-T_0$ and $+T_0$, respectively, as shown in Fig. 3. And the other four walls are adiabatic, i.e., $\partial_{\hat{n}} T = 0$ at these walls, where $\hat{\boldsymbol{n}}$ is the unit vector out-normal to a wall. The gravitation is pointing downward ($-\hat{\boldsymbol{y}}$ direction). The Rayleigh number Ra is defined as

$$\text{Ra} = \frac{2T_0 g \beta \gamma L^3}{\nu \kappa_{\text{eff}}} = \text{Pr} \cdot \text{Gr}, \tag{45}$$

where g is the gravitational acceleration, β ($= -\partial_T \ln \rho|_p$) is the coefficient of thermal expansion, $L = N_x = 50$ in the simulations, and $\text{Gr} = 2T_0 g \beta \gamma L^3/\nu^3$ is the Grashof number. Two effective Nusselt numbers are defined for the flow. The effective local Nusselt number Nu_w is defined by the temperature gradient at the wall maintained at a constant temperature:

$$\text{Nu}_w = \frac{1}{2T_0 L_z} \sum_{y,z} \partial_x T \big|_{x=1/2}, \tag{46}$$

where $L_z = N_z$ in the lattice units. The effective (volume) averaged Nusselt number Nu_v is defined as

$$\text{Nu}_v = \frac{1}{2T_0 \kappa_{\text{eff}} L L_z} \sum_{x,y,z} u_x T - 1, \tag{47}$$

where $\kappa_{\text{eff}} = \kappa/\gamma$. In the simulations, we use the following parameters: $\gamma = 1.2$, $\nu = 0.06$, $\text{Pr} = 0.71$ (for air), and T_0
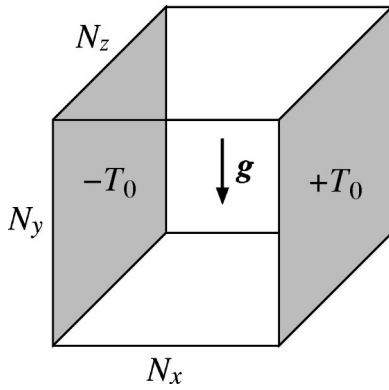
FIG. 3. Geometry of rectangular cavity. Two shaded opposite vertical walls are maintained with constant temperatures $-T_0$ and $+T_0$, respectively. The temperature boundary conditions on other four (transparent) walls are $\partial_{\hat{n}} T = 0$—the adiabatic boundary conditions.

FIG. 4. Effective Nusselt number Nu as a function of the cavity length $L_z = N_z$. The solid and dashed curves correspond to the volume measurement Nu_v and the local measurement at wall, Nu_w, respectively. The relative differences $(Nu^* - Nu)/Nu^*$ are plotted for $Nu_* = 4.337$ at $Ra = 10^5$ and $Nu^* = 8.640$ at $Ra = 10^6$ obtained by using a pseudospectral method [66].

$=1$, all in lattice units. Bear in mind that we can reduce the system size by half by using the 13-velocity model because of the parity conservation of the model.

We use two values of the effective Rayleigh number Ra $= 10^5$ and 10^6 (corresponding to $g\beta \approx 2.028 \times 10^{-3}$ and 2.028×10^{-2}, respectively), and compute the two effective Nusselt numbers Nu_w and Nu_v, as defined above. As $L_z \rightarrow \infty$, the flow becomes quasi-two-dimensional. The two effective Nusselt numbers obtained are $Nu_w = 4.27$ and $Nu_v = 8.31$, compared to 4.337 and 8.640 obtained by an accurate pseudospectral method [66]. Figure 4 shows the effective Nusselt numbers Nu_w and Nu_v, respectively, normalized by 4.337 and 8.640 for $Ra = 10^5$ and 10^6, as functions of the length of the cavity (L_z). The difference between the present results and that of Ref. [66] is partially due to the fact that the lattice Boltzmann equation simulates weakly compressible fluids, whereas the pseudospectral method used in Ref. [66] solves the incompressible Navier-Stokes equations. In fact, for $Ra = 10^6$, the magnitude of the mean velocity in the cavity is about 0.081, which is not negligible compared to the speed of sound ($c_s = 0.456$) for the model (the mean Mach number Ma ≈ 0.18). A detailed convergence study of the numerical scheme is presented elsewhere [67].

VI. CONCLUSION

In this paper we propose to solve the thermohydrodynamic equations by using a hybrid lattice Boltzmann scheme: the usual lattice Boltzmann equation is used to solve the mass and momentum conservation equations, while a finite-difference method is used to solve the diffusion-advection equation satisfied by the temperature, with appropriate couplings between the two systems. A number of hybrid models in both two and three dimensions are analyzed and compared with the energy-conserving TLBE models. The rationale behind our proposal is based on the analysis of the existing energy-conserving TLBE models that suffer such severe numerical instabilities that their applicabilities are much limited. We have identified that a main defect in the existing energy-conserving TLBE models is the coupling be-
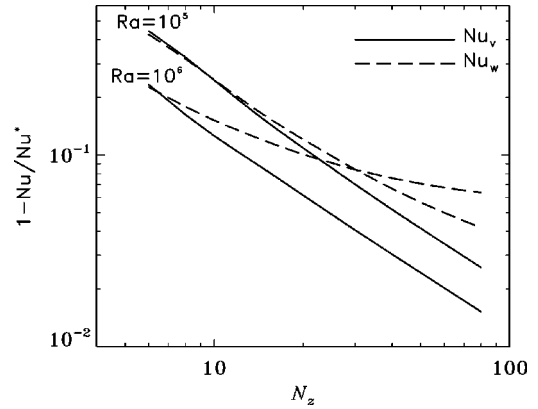
tween the energy and shear modes of the linearized LBE evolution operator. This coupling is nonphysical and inherent to all the existing energy-conserving TLBE models. This spurious coupling is forbidden in a continuum model because it violates rotational symmetry (isotropy), but occurs in a discrete model that is inherently anisotropic beyond certain order in $\mathbf{k}$. The hybrid thermal lattice Boltzmann method eliminates this unphysical coupling and significantly improves the numerical stability. The hybrid TLBE model is almost as stable as the athermal lattice Boltzmann equation without the temperature equation, provided that the appropriate finite-difference stencils with the same symmetry as the discrete velocities are used.

Similar to our previous work [45], we analyze the effects of interpolations. In general, second- or higher-order spatial interpolations applied to the distribution functions do not affect the values of the transport coefficients, the isotropy, and Galilean invariance of the LBE system at the $\mathbf{k}=\mathbf{0}$ limit; therefore they do not affect the large scale hydrodynamics. However, interpolations do introduce significant numerical viscosities, especially in small scales comparable to the lattice spacing. The numerical viscosities dissipate small scale fluctuations, and therefore improve the numerical stability. Second, the interpolations used in the LBE schemes usually have a symmetry different from (often much less than) that of the discrete velocity set, therefore they alter the overall symmetry properties (the isotropy and Galilean invariance) of the LBE scheme. Again, this effect is especially severe at small scales. And finally, interpolations destroy the local conservation laws. Therefore, interpolations should be used with care.

The present work differs from the existing ones in several aspects. First, we advocate the multiple-relaxation-time (MRT) model as opposed to the simple BGK approximation which is in part responsible for numerical instabilities in the existing LBE models. Besides the improvement of the numerical stability, the Prandtl number is adjustable for the MRT models, while the Prandtl number is fixed to unity for

the BGK models. Second, we have provided a systematic analysis of the proposed HTLBE model, and a comparative study to the energy-conserving TLBE models. The thermal and acoustic properties of various models are analyzed in detail. The analysis immediately offers insight into the short-comings of the existing TLBE models. We conclude that many existing models gain numerical stability by using interpolations at the expense of isotropy and relatively low numerical viscosities. Finally, the HTLBE model studied here does not use Boussinesq approximation explicitly. It can be extended to situations where Boussinesq approximation does not apply by including nonlinear terms related to compressible effects and using temperature-dependent transport coefficients. It should also be noted that the proposed HTLBE scheme is only applicable for low/moderate Mach number flows. This is an inherent limitation due to the LBE models with polynomial equilibria, and the MRT models are not exceptions in this regard.

It must be cautioned that our proposal to use the hybrid method is not the final solution of the approach based on the thermal lattice Boltzmann equation. This approach significantly deviates from the orthodox lattice Boltzmann methodology based on the kinetic theory, and it only provides a compromised solution. The difficulty encountered in the lattice Boltzmann equation is that we have not been able to come up with an effective way to mimic temperature "statistically" based on kinetic theory and still be as efficient as the macroscopic approach. The reason that the lattice Boltzmann equation is much more successful in handling the mass and momentum conservation laws is that one does not need to deal with any quantity which is statistical in nature, such as the temperature. Several issues remain to be addressed. First, the factor γ in the advection term of the T equation is undesirable. However, the effect of this only amounts to the rescaling of κ to $\kappa_{eff} = \kappa/\gamma$, as shown in the analysis and simulations. Second, the isothermal sound speed is independent of the temperature T. The validity of the linear analysis suggests that the relaxation type of the collision model in the lattice Boltzmann equation may not have sufficient nonlinearity to mimic the thermal phenomena and needs severe modifications. And third, we have not considered the nonlinear dissipation terms in the temperature equation. However, within the HTLBE framework, including these nonlinear terms, is in principle, as easy as considering a more complicated dynamics for T for more complex situations, and this is indeed one of the useful features of hybrid models. These open questions are left for future work.

Based on the framework in the present work, the methodology of the hybrid lattice Boltzmann scheme can be readily extended to other systems, such as fluids of multiple components with different diffusion coefficients (cf. Ref. [69] and references therein), and non-Newtonian fluids [70,71].

APPENDIX A: CONSTRUCTION OF TRANSFORMATION MATRIX ON 2D SQUARE LATTICES OR 3D CUBIC LATTICES

The construction of the transformation matrix M is very closely related to the definition of moments used in kinetic theory of gases (e.g., Ref. [68]). The main difference is due to the absence of a weight factor in the LBE method similar to the Maxwellian equilibrium in the evaluation of an average (i.e., a weighted norm). In addition, degeneracies of moments arise due to the small number of geometrically symmetrically collocated discrete velocities used in the LBE method. For example, for a model with only unit speed (the D2Q6, D2Q7, or models with the single-speed "octagonal" velocity set), moments of $(c_{ix}^2 + c_{iy}^2)^m$ are all equal for $m \geq 1$, leading to the absence of these moments which exist in real gases. This can produce anisotropic behavior of the model.

The considerations to uniquely determine the orthogonal basis vectors spanning the transformation matrix M are the following. First, it is coordinate system dependent. The coordinates used here are that of Cartesian coordinates (x, y) in 2D and (x, y, z) in 3D. And some or all of the unit-speed velocities are always aligned with the coordinate axes. Second, the normalization of the vectors is arbitrary, and the normalization used here is that the components of the vectors are minimal integers to simplify algebraic manipulations. And third, symmetry properties of the moments are fully exploited, as discussed in the following. This simplifies derivations and leads naturally to moments with a clear physical significance, which are particularly suited for the purpose of modeling the dynamics of an isotropic fluid.

For square lattices in two dimensions, the construction of the transformation matrix M can be greatly simplified by observing that for symmetry reasons nonzero velocities $\{c_i \neq 0\}$ are usually added in groups of four velocities of equal speed, i.e., the axial velocities of integer speeds, and/or the diagonal velocities of speeds in multiples of $\sqrt{2}$. Both the axial and diagonal velocities contribute to the density mode $\langle \rho |$ equally, but one nontrivial moment of a group of four axial velocities only contributes to mode $\langle p_{xx} | \propto \langle (j_x^2 - j_y^2) |$, whereas that of four equal-speed diagonal velocities only contributes to mode $\langle p_{xy} | \propto \langle j_x j_y |$, and these two modes are linearly independent. Thus, the transformation matrix M can be constructed from the subspaces of the zero velocity, the group of axial velocities, and the group of diagonal velocities. Specifically, for the D2Q9S model the two subspaces of axial and diagonal velocities are

$$\mathsf{M}^{(a)} = \begin{pmatrix} \langle \rho | \\ \langle j_x | \\ \langle j_y | \\ \langle p_{xx} | \end{pmatrix} = \begin{pmatrix} 1 & 1 & 1 & 1 \\ 1 & 0 & -1 & 0 \\ 0 & 1 & 0 & -1 \\ 1 & -1 & 1 & -1 \end{pmatrix}, \quad \text{(A1a)}$$

$$
\mathsf{M}^{(d)} = \begin{pmatrix} \langle\rho| \\ \langle j_x| \\ \langle j_y| \\ \langle p_{xy}| \end{pmatrix} = \begin{pmatrix} 1 & 1 & 1 & 1 \\ 1 & -1 & -1 & 1 \\ 1 & 1 & -1 & -1 \\ 1 & -1 & 1 & -1 \end{pmatrix}. \quad \text{(A1b)}
$$

We further note that, under the elementary transformations of a square on the plane,

$$x \rightarrow -x, \quad \text{(A2a)}$$

$$y \rightarrow -y, \quad \text{(A2b)}$$

$$(x,y) \rightarrow (y,x), \quad \text{(A2c)}$$

the row vectors in $\mathsf{M}^{(a)}$ and $\mathsf{M}^{(d)}$ have the following behavior: $\langle\rho|$'s behave as a scalar, $\langle j_x|$'s and $\langle j_y|$'s behave as a vector component, and $\langle p_{xx}|$'s and $\langle p_{xy}|$'s behave as components of a second-rank tensor. These orthogonal 4×4 subspaces provide the building blocks of the transformation matrix M for the model with axial and diagonal velocities, and when constructing M, only the modes with the same symmetry can be coupled to each other. When there are more than one speed in either groups of axial and/or diagonal velocities, we may first determine the number of moments of each symmetry, in order to partition the Gram-Schmidt process in independent subprocesses. For instance, consider a 13-velocity model on square lattice (D2Q13S), there are four scalar moments for ρ, three vector moments for j_x and three for j_y, two second-rank tensor moments for p_{xx}, and only one for p_{xy}. Orthogonalization should be carried out successively for groups of four $\langle\rho|$'s, three $\langle j_x|$'s, three $\langle j_y|$'s, two $\langle p_{xx}|$'s, and one $\langle p_{xy}|$. Similar considerations based on symmetry are also applied in the construction of the equilibria of the moments, because couplings can only be allowed for those quantities in each velocity class (group) which behave exactly the same under the 2D transformations defined by Eqs (A2). To be more explicit, the moments can be related to some elementary polynomials defined on a 2D lattice. That is, for the zero velocity, it is 1. For four equal-speed axial velocities, they are 1, x, y, and (x^2-y^2). And for four equal-speed diagonal velocities, they are 1, x, y, and xy. By applying the Gram-Schmidt procedure to the elementary polynomials and their appropriate combinations, we immediately obtain the orthogonal polynomials (Table VI). By considering up to fourth- and sixth-order polynomials, we obtain the orthogonal polynomials for the D2Q9S and D2Q13S models, respectively. Obviously, the orthogonal polynomials for the D2Q13S model include those for the D2Q9S model. (Note that in Table VI, x and y are used instead of c_{ix} and c_{iy}.)

We now apply the same symmetry consideration to models on 3D cubic lattices. On a basic cubic lattice, we consider four groups of velocities classified by their speeds: 0 (the center of the cube), 1 (six surfaces), $\sqrt{2}$ (12 edges), and $\sqrt{3}$ (eight corners). The zero velocity can only describe a scalar, i.e., 1—the zeroth order moment. The six velocities of speed 1 can describe a scalar, a vector, and part of second-rank

TABLE VI. The orthogonal polynomials obtained from the elementary polynomials of $\{1, x, y, xy, (x^2-y^2)\}$ via the Gram-Schmidt procedure for the D2Q9S and D2Q13S models. The orthogonal polynomials for the D2Q13S model must also include those for the D2Q9S model.

	D2Q9S	D2Q13S
Scalars	1, (x^2+y^2), $(x^2+y^2)^2$	$(x^2+y^2)^3$
Vectors	x, $x(x^2+y^2)$	$x(x^2+y^2)^2$
	y, $y(x^2+y^2)$	$y(x^2+y^2)^2$
Tensors	(x^2-y^2)	$(x^2-y^2)(x^2+y^2)$
	xy	

tensor. Similarly, the 12 velocities of speed $\sqrt{2}$ can describe a scalar, a vector, a second-rank tensor, and part of a third-rank tensor, whereas the eight velocities of speed $\sqrt{3}$ can describe a scalar, a vector, part of a second-rank tensor, and part of a third rank tensor. The elementary polynomials corresponding to each velocity group are given in Table VII. The D3Q13 model uses the velocities of 0 and $\sqrt{2}$ speeds, the D3Q15 model uses the velocities of 0, 1, and $\sqrt{3}$ speeds, the D3Q19 model uses the velocities of 0, 1, and $\sqrt{2}$ speeds, and the D3Q27 model uses all the 27 velocities of 0, 1, $\sqrt{2}$, and $\sqrt{3}$ speeds. Starting with these elementary polynomials, the transformation matrices for the 3D models can be easily obtained via the Gram-Schmidt procedure. To reproduce correct incompressible hydrodynamic equations in 3D, one needs the five components of a symmetric traceless second-rank tensor (the stress). It thus becomes obvious why the minimal model in 3D is D3Q13, and that D3Q15 or D3Q19 would also work, as indicated by the polynomials shown in Table VII.

APPENDIX B: LINEAR ANALYSIS AND HYDRODYNAMIC BEHAVIOR OF ATHERMAL LBE

For athermal lattice Boltzmann models with $(b+1)$ velocities on a lattice of N nodes in D dimensions, there are $(D+1)$ local conserved modes, and thus $(b-D) = (b+1) - (D+1)$ local (nonconserved) "slave" modes. The local slave modes evolve with time scales of the order of $1/s_i$, $i = (D+2), \ldots, (b+1)$ (s_i is the relaxation rate). The collision enforces the local conservation laws, while the advection preserves the global conservation laws when there are no boundaries. Although the conserved modes are not changed by the collision, they are nevertheless affected by the "slave" modes, because the fluxes of some of the conserved modes are related to these nonconserved quantities. Emerging from the evolution of collision and advection are the long-time and large-scale hydrodynamic behavior which can be described by a set of partial differential equations (the Navier-Stokes equations). The Navier-Stokes equations (or the long-time and large-scale hydrodynamic behavior) can be derived from such a system via the Chapman-Enskog analysis, or equivalently, via the mode analysis of the dispersion equation (von Neumann analysis) [45].

TABLE VII. Twenty-seven discrete velocities and the corresponding elementary polynomials on a 3D cubic lattice.

Speed	Polynomial	Rank
0	1	0
	1	0
1	x, y, z	1
	$4x^2 - (x^2+y^2+z^2)$, (y^2-z^2)	2
	1	0
	x, y, z	1
$\sqrt{2}$	$4x^2 - (x^2+y^2+z^2)$, (y^2-z^2), xy, yz, zx	2
	$x(y^2-z^2)$, $y(z^2-x^2)$, $z(x^2-y^2)$	3
	1	0
	x, y, z	1
$\sqrt{3}$	xy, yz, zx	2
	xyz	3

We can linearize the evolution equation (1) around the state with a constant velocity V to obtain a linearized equation for the fluctuations δf in Fourier space [45]:

$$|\delta f(\boldsymbol{k}, t+1)\rangle = \mathsf{L}|\delta f(\boldsymbol{k}, t)\rangle, \tag{B1a}$$

$$\mathsf{L} = \mathsf{A}^{-1}[\mathsf{I} + \mathsf{M}^{-1}\mathsf{CM}], \tag{B1b}$$

where I is the identity matrix, C is the linearized collision operator, and A is the propagation operator that is a diagonal matrix in the space of $|f\rangle$:

$$\mathsf{A} = \mathrm{diag}(e^{-i\boldsymbol{k}\cdot\boldsymbol{c}_0}, e^{-i\boldsymbol{k}\cdot\boldsymbol{c}_1}, \dots, e^{-i\boldsymbol{k}\cdot\boldsymbol{c}_b}).$$

For the LBE schemes with interpolations and/or extrapolations, A is no longer a diagonal matrix, its band structure depends on the interpolation/extrapolation stencils (cf. Ref. [45]). The solution of the eigenvalue problem of the linearized evolution operator,

$$\mathsf{L}|\varphi\rangle = z|\varphi\rangle, \tag{B2}$$

yields the generalized hydrodynamics of the model, i.e., the $\boldsymbol{k}$ dependence of the transport coefficients, the sound speed, and the Galilean-invariance factor g [45,72]. Note that the instability corresponds to the positivity of the real part of $\ln z$, which usually appears at fairly large values of k when the mean velocity of the flow increases.

Usually, the eigenvalue equation (B2) of L (the dispersion equation) does not have analytic solutions. But it can be solved perturbatively in $\boldsymbol{k}$ [45,72]. For athermal lattice Boltzmann models in two dimensions, which only need to satisfy mass and momentum conservation laws, there are only three hydrodynamic modes: one transverse mode (the vorticity) $m_\perp$ and two longitudinal modes (sound waves) $m_\pm$. These hydrodynamic modes are the three-fold degenerated eigenmodes of L with a unity eigenvalue at $\boldsymbol{k}=\boldsymbol{0}$ [45,72]. For a two-dimensional system with a uniform velocity V and a small density fluctuation of wave-vector $\boldsymbol{k}$, and subjected to periodic boundary conditions, linear analysis of the dispersion equation yields the following results to the first order in V and second order in $\boldsymbol{k}$ [45,72]:

$$m_\perp(\boldsymbol{k}, t) = \exp(-i\boldsymbol{k}\cdot\boldsymbol{V}t - \nu k^2 t)m_\perp(0), \tag{B3a}$$

$$m_\pm(\boldsymbol{k}, t) = \exp\left(-i(\boldsymbol{k}\cdot\boldsymbol{V} \pm kc_s)t - \frac{1}{2}(\nu+\zeta)k^2 t\right)m_\pm(0), \tag{B3b}$$

where $m_\perp(0)$ and $m_\pm(0)$ are initial amplitudes of these modes, ν and ζ are, respectively, the shear and bulk kinematic viscosities, and c_s is the sound speed of the model. The terms linear in V in the above results are due to the nonlinear advection, and they can be viewed as the manifestation of *Galilean invariance* of the model.

Besides the underlying lattice structure, the sound speed and the transport coefficients depend on the equilibria $\{m_i^{(eq)}\}$ and the relaxation rates $\{s_i\}$. It is important to make certain that the sound speed c_s and transport coefficients ν and ζ are independent of the orientation of wave vector $\boldsymbol{k}$ with respect to the underlying lattice structure, that is, the model has to be isotropic. The Galilean invariance and isotropy of the LBE model are attained by carefully choosing parameters in the model via a linear analysis [45]. When solving the dispersion equation (B2) perturbatively in power of $\boldsymbol{k}$, the first-order and the second-order solutions lead to the sound speed c_s and Galilean factor g, and the attenuation coefficients (which are combinations of the transport coefficients), respectively, as functions of relaxation rates $\{s_i\}$ and other adjustable parameters in the equilibria $\{m_i^{(eq)}\}$. This analysis is systematically used to determine the optimal values of the parameters.

APPENDIX C: STENCILS OF D2Q9S MODEL

The stencils for the gradient ∇ and the Laplacian operators Δ for the D2Q9S model are constructed as follows. The following $B\ (=b+1)$ number of polynomials:

$$\varphi_0 = 1, \tag{C1a}$$

$$\varphi_1 = x, \quad \varphi_2 = y, \tag{C1b}$$

$$\varphi_3 = (x^2 - y^2), \quad \varphi_4 = xy, \quad \varphi_5 = (x^2 + y^2), \tag{C1c}$$

$$\varphi_6 = x(x^2 + y^2), \quad \varphi_7 = y(x^2 + y^2), \tag{C1d}$$

$$\varphi_8 = (x^2 + y^2)^2, \tag{C1e}$$

are used to expand a function $f(x,y)$ in two-dimensional space,

$$f(x,y) = \sum_{i=0}^{b} a_i \varphi_i. \tag{C2}$$

The coefficients $\{a_i | i = 0, 1, \ldots, b\}$ are determined by B values of $f(x,y)$ at the point (x,y) and other points in its vicin-ity defined by the discrete velocity set on the lattice space. Specifically, these points are $(0,0)$, $(\pm 1,0)$, $(0,\pm 1)$, and $(\pm 1,\pm 1)$ for the D2Q9S model. The derivatives of $f(x,y)$ are obtained from Eq. (C2) by taking differentiations with respect to appropriate variables. The finite-difference operators obtained this way for the D2Q9S model are

$$\partial_x^* f(i,j) = f(i+1,j) - f(i-1,j) - \frac{1}{4}[f(i+1,j+1) \\ - f(i-1,j+1) + f(i+1,j-1) - f(i-1,j-1)],$$

$$\partial_y^* f(i,j) = f(i,j+1) - f(i,j-1) - \frac{1}{4}[f(i+1,j+1) \\ - f(i+1,j-1) + f(i-1,j+1) - f(i-1,j-1)],$$

$$\Delta^* f(i,j) = 2[f(i+1,j) + f(i-1,j) + f(i,j+1) + f(i,j-1)] \\ - \frac{1}{2}[f(i+1,j+1) + f(i-1,j+1) + f(i-1,j-1) \\ + f(i+1,j-1)] - 6f(i,j).$$

APPENDIX D: TRANSFORMATION MATRIX AND STENCILS FOR D3Q13 MODEL

The transformation matrix M for the 13-velocity model in 3D (D3Q13) [49] is

$$
\begin{pmatrix} \langle \rho | \\ \langle j_x | \\ \langle j_y | \\ \langle j_z | \\ \langle e | \\ \langle 3p_{xx} | \\ \langle p_{ww} | \\ \langle p_{xy} | \\ \langle p_{yz} | \\ \langle p_{zx} | \\ \langle \varphi_x | \\ \langle \varphi_y | \\ \langle \varphi_z | \end{pmatrix}
=
\begin{pmatrix}
1 & 1 & 1 & 1 & 1 & 1 & 1 & 1 & 1 & 1 & 1 & 1 & 1 \\
0 & 1 & -1 & 1 & -1 & 0 & 0 & 0 & 0 & 1 & 1 & -1 & -1 \\
0 & 1 & 1 & -1 & -1 & 1 & -1 & 1 & -1 & 0 & 0 & 0 & 0 \\
0 & 0 & 0 & 0 & 0 & 1 & 1 & -1 & -1 & 1 & -1 & 1 & -1 \\
-12 & 1 & 1 & 1 & 1 & 1 & 1 & 1 & 1 & 1 & 1 & 1 & 1 \\
0 & 1 & 1 & 1 & 1 & -2 & -2 & -2 & -2 & 1 & 1 & 1 & 1 \\
0 & 1 & 1 & 1 & 1 & 0 & 0 & 0 & 0 & -1 & -1 & -1 & -1 \\
0 & 1 & -1 & -1 & 1 & 0 & 0 & 0 & 0 & 0 & 0 & 0 & 0 \\
0 & 0 & 0 & 0 & 0 & 1 & -1 & -1 & 1 & 0 & 0 & 0 & 0 \\
0 & 0 & 0 & 0 & 0 & 0 & 0 & 0 & 0 & 1 & -1 & -1 & 1 \\
0 & 1 & -1 & 1 & -1 & 0 & 0 & 0 & 0 & -1 & -1 & 1 & 1 \\
0 & -1 & -1 & 1 & 1 & 1 & -1 & 1 & -1 & 0 & 0 & 0 & 0 \\
0 & 0 & 0 & 0 & 0 & -1 & -1 & 1 & 1 & 1 & -1 & 1 & -1
\end{pmatrix}. \tag{D1}
$$

The stencils for the gradient ∇ and the Laplacian operators Δ are given as the following for the D3Q13 model. Only the ∂_x^* and Δ^* are given because ∂_y^* and ∂_z^* can be easily constructed based on ∂_x^*. The polynomials used to obtain the finite-difference operators are

$$\varphi_0 = 1, \tag{D2a}$$

$$\varphi_1 = x, \quad \varphi_2 = y, \quad \varphi_3 = z, \tag{D2b}$$

$$\varphi_4 = (x^2 + y^2 + z^2), \quad \varphi_5 = (2x^2 - y^2 - z^2),$$

$$\varphi_6 = (x^2 - y^2), \quad \varphi_7 = xy, \quad \varphi_8 = yz, \quad \varphi_9 = zx, \tag{D2c}$$

$$\varphi_{10} = x(y^2 - z^2), \quad \varphi_{11} = y(z^2 - x^2), \quad \varphi_{12} = z(x^2 - y^2). \tag{D2d}$$

The finite-difference operators are

$$\partial_x^* f(i,j,k) = \frac{1}{8}[f(i+1,j+1,k) - f(i-1,j+1,k)$$
$$+ f(i+1,j-1,k) - f(i-1,j-1,k)$$
$$+ f(i+1,j,k+1) - f(i-1,j,k+1)$$
$$+ f(i+1,j,k-1) - f(i-1,j,k-1)],$$

$$\Delta^* f(i,j,k) = \frac{1}{4}[f(i+1,j+1,k) + f(i-1,j+1,k)$$
$$+ f(i+1,j-1,k) + f(i-1,j-1,k)$$
$$+ f(i,j+1,k+1) + f(i,j-1,k+1)$$
$$+ f(i,j+1,k-1) + f(i,j-1,k-1)$$
$$+ f(i+1,j,k+1) + f(i-1,j,k+1)$$
$$+ f(i+1,j,k-1) + f(i-1,j,k-1)]$$
$$- 3f(i,j,k).$$

APPENDIX E: TRANSFORMATION MATRIX AND STENCILS OF D3Q15 MODEL

The transformation matrix M for the 15-velocity model in 3D (D3Q15) is

$$
\begin{pmatrix} \langle\rho| \\ \langle e| \\ \langle\epsilon| \\ \langle j_x| \\ \langle q_x| \\ \langle j_y| \\ \langle q_y| \\ \langle j_z| \\ \langle q_z| \\ \langle 3p_{xx}| \\ \langle p_{ww}| \\ \langle p_{xy}| \\ \langle p_{yz}| \\ \langle p_{zx}| \\ \langle\psi_{xyz}| \end{pmatrix}
=
\begin{pmatrix}
1 & 1 & 1 & 1 & 1 & 1 & 1 & 1 & 1 & 1 & 1 & 1 & 1 & 1 & 1 \\
-2 & -1 & -1 & -1 & -1 & -1 & -1 & 1 & 1 & 1 & 1 & 1 & 1 & 1 & 1 \\
16 & -4 & -4 & -4 & -4 & -4 & -4 & 1 & 1 & 1 & 1 & 1 & 1 & 1 & 1 \\
0 & 1 & -1 & 0 & 0 & 0 & 0 & 1 & -1 & 1 & -1 & 1 & -1 & 1 & -1 \\
0 & -4 & 4 & 0 & 0 & 0 & 0 & 1 & -1 & 1 & -1 & 1 & -1 & 1 & -1 \\
0 & 0 & 0 & 1 & -1 & 0 & 0 & 1 & 1 & -1 & -1 & 1 & 1 & -1 & -1 \\
0 & 0 & 0 & -4 & 4 & 0 & 0 & 1 & 1 & -1 & -1 & 1 & 1 & -1 & -1 \\
0 & 0 & 0 & 0 & 0 & 1 & -1 & 1 & 1 & 1 & 1 & -1 & -1 & -1 & -1 \\
0 & 0 & 0 & 0 & 0 & -4 & 4 & 1 & 1 & 1 & 1 & -1 & -1 & -1 & -1 \\
0 & 2 & 2 & -1 & -1 & -1 & -1 & 0 & 0 & 0 & 0 & 0 & 0 & 0 & 0 \\
0 & 0 & 0 & 1 & 1 & -1 & -1 & 0 & 0 & 0 & 0 & 0 & 0 & 0 & 0 \\
0 & 0 & 0 & 0 & 0 & 0 & 0 & 1 & -1 & -1 & 1 & 1 & -1 & -1 & 1 \\
0 & 0 & 0 & 0 & 0 & 0 & 0 & 1 & 1 & -1 & -1 & -1 & -1 & 1 & 1 \\
0 & 0 & 0 & 0 & 0 & 0 & 0 & 1 & -1 & 1 & -1 & -1 & 1 & -1 & 1 \\
0 & 0 & 0 & 0 & 0 & 0 & 0 & 1 & -1 & -1 & 1 & -1 & 1 & 1 & -1
\end{pmatrix}.
$$

The finite-difference operators are

$$\partial_x^* f(i,j,k) = \frac{3}{4}[f(i+1,j,k) - f(i-1,j,k)] - \frac{1}{16}[f(i+1,j+1,k+1) - f(i-1,j+1,k+1) + f(i+1,j-1,k+1)$$
$$- f(i-1,j-1,k+1) + f(i+1,j+1,k-1) - f(i-1,j+1,k-1) + f(i+1,j-1,k-1) - f(i-1,j-1,k-1)],$$

$$\Delta^* f(i,j,k) = \frac{3}{2}[f(i+1,j,k) + f(i-1,j,k) + f(i,j+1,k) + f(i,j-1,k) + f(i,j,k+1) + f(i,j,k-1)]$$

$$- \frac{1}{8}[f(i+1,j+1,k+1) + f(i-1,j+1,k+1) + f(i+1,j-1,k+1) + f(i-1,j-1,k+1) + f(i+1,j+1,k-1)$$

$$+ f(i-1,j+1,k-1) + f(i+1,j-1,k-1) + f(i-1,j-1,k-1)] - 8f(i,j,k).$$

APPENDIX F: TRANSFORMATION MATRIX OF D3Q19 MODEL

The transformation matrix M for the 19-velocity model in 3D (D3Q19) model is

$$
\begin{pmatrix}
1 & 1 & 1 & 1 & 1 & 1 & 1 & 1 & 1 & 1 & 1 & 1 & 1 & 1 & 1 & 1 & 1 & 1 & 1 \\
-30 & -11 & -11 & -11 & -11 & -11 & -11 & 8 & 8 & 8 & 8 & 8 & 8 & 8 & 8 & 8 & 8 & 8 & 8 \\
12 & -4 & -4 & -4 & -4 & -4 & -4 & 1 & 1 & 1 & 1 & 1 & 1 & 1 & 1 & 1 & 1 & 1 & 1 \\
0 & 1 & -1 & 0 & 0 & 0 & 0 & 1 & -1 & 1 & -1 & 1 & -1 & 1 & -1 & 0 & 0 & 0 & 0 \\
0 & -4 & 4 & 0 & 0 & 0 & 0 & 1 & -1 & 1 & -1 & 1 & -1 & 1 & -1 & 0 & 0 & 0 & 0 \\
0 & 0 & 0 & 1 & -1 & 0 & 0 & 1 & 1 & -1 & -1 & 0 & 0 & 0 & 0 & 1 & -1 & 1 & -1 \\
0 & 0 & 0 & -4 & 4 & 0 & 0 & 1 & 1 & -1 & -1 & 0 & 0 & 0 & 0 & 1 & -1 & 1 & -1 \\
0 & 0 & 0 & 0 & 0 & 1 & -1 & 0 & 0 & 0 & 0 & 1 & 1 & -1 & -1 & 1 & 1 & -1 & -1 \\
0 & 0 & 0 & 0 & 0 & -4 & 4 & 0 & 0 & 0 & 0 & 1 & 1 & -1 & -1 & 1 & 1 & -1 & -1 \\
0 & 2 & 2 & -1 & -1 & -1 & -1 & 1 & 1 & 1 & 1 & 1 & 1 & 1 & 1 & -2 & -2 & -2 & -2 \\
0 & -4 & -4 & 2 & 2 & 2 & 2 & 1 & 1 & 1 & 1 & 1 & 1 & 1 & 1 & -2 & -2 & -2 & -2 \\
0 & 0 & 0 & 1 & 1 & -1 & -1 & 1 & 1 & 1 & 1 & -1 & -1 & -1 & -1 & 0 & 0 & 0 & 0 \\
0 & 0 & 0 & -2 & -2 & 2 & 2 & 1 & 1 & 1 & 1 & -1 & -1 & -1 & -1 & 0 & 0 & 0 & 0 \\
0 & 0 & 0 & 0 & 0 & 0 & 0 & 1 & -1 & -1 & 1 & 0 & 0 & 0 & 0 & 0 & 0 & 0 & 0 \\
0 & 0 & 0 & 0 & 0 & 0 & 0 & 0 & 0 & 0 & 0 & 0 & 0 & 0 & 0 & 1 & -1 & -1 & 1 \\
0 & 0 & 0 & 0 & 0 & 0 & 0 & 0 & 0 & 0 & 0 & 1 & -1 & -1 & 1 & 0 & 0 & 0 & 0 \\
0 & 0 & 0 & 0 & 0 & 0 & 0 & 1 & -1 & 1 & -1 & -1 & 1 & -1 & 1 & 0 & 0 & 0 & 0 \\
0 & 0 & 0 & 0 & 0 & 0 & 0 & -1 & -1 & 1 & 1 & 0 & 0 & 0 & 0 & 1 & -1 & 1 & -1 \\
0 & 0 & 0 & 0 & 0 & 0 & 0 & 0 & 0 & 0 & 0 & 1 & 1 & -1 & -1 & -1 & -1 & 1 & 1
\end{pmatrix}.
$$

The row vector of M is ordered as $\langle\rho|$, $\langle e|$, $\langle\varepsilon|$, $\langle j_x|$, $\langle q_x|$, $\langle j_y|$, $\langle q_y|$, $\langle j_z|$, $\langle q_z|$, $\langle 3p_{xx}|$, $\langle 3\pi_{xx}|$, $\langle p_{ww}|$, $\langle\pi_{ww}|$, $\langle p_{xy}|$, $\langle p_{yz}|$, $\langle p_{xz}|$, $\langle\varphi_x|$, $\langle\varphi_y|$, and $\langle\varphi_z|$, where $\langle 3\pi_{xx}|$ and $\langle\pi_{ww}|$ are fourth-order moments, and $\langle\varphi_x|$, $\langle\varphi_y|$, and $\langle\varphi_z|$ are third-order moments [50].

The finite-difference operators are

$$
\partial_x^* f(i,j,k) = f(i+1,j,k) - f(i-1,j,k) - \frac{1}{8}[f(i+1,j+1,k) - f(i-1,j+1,k) + f(i+1,j-1,k) - f(i-1,j-1,k)
$$

$$
+ f(i+1,j,k+1) - f(i-1,j,k+1) + f(i+1,j,k-1) - f(i-1,j,k-1)],
$$

$$
\Delta^* f(i,j,k) = 2[f(i+1,j,k) + f(i-1,j,k) + f(i,j+1,k) + f(i,j-1,k) + f(i,j,k+1) + f(i,j,k-1)]
$$

$$
- \frac{1}{4}[f(i+1,j+1,k) + f(i-1,j+1,k) + f(i+1,j-1,k) + f(i-1,j-1,k) + f(i,j+1,k+1)
$$

$$
+ f(i,j-1,k+1) + f(i,j+1,k-1) + f(i,j-1,k-1) + f(i+1,j,k+1) + f(i-1,j,k+1)
$$

$$
+ f(i+1,j,k-1) + f(i-1,j,k-1)] - 9f(i,j,k).
$$

APPENDIX G: ANALYSIS OF THE 2D LBE MODEL WITH AN OCTAGONAL VELOCITY SET AND INTERPOLATIONS

This appendix provides an analysis for the lattice Boltzmann model with "octagonal" velocity sets [27–32]. For the sake of simplicity, we restrict our analysis to the model with nine velocities, i.e, one zero velocity and eight velocities of unit speed. With the same notations as in Appendix A, we have

$$
\langle j_x| = (0,1,\varpi,0,-\varpi,-1,-\varpi,0,\varpi)r, \tag{G1a}
$$

$$
\langle j_y| = (0,0,\varpi,1,\varpi,0,-\varpi,-1,-\varpi)r, \tag{G1b}
$$

where $\varpi = 1/\sqrt{2}$, and the labeling of the velocities is 0 for the zero velocity c_0, and c_i ($i = 1-8$) for nonzero velocities, starting with c_1 along the x axis in the counterclockwise order. The parameter r is introduced for the sake of generality: when $r = 1$ (which is the athermal model using the velocity set presented in Ref. [27]), the velocities along the axial directions, i.e., $c_{1,3,5,7}$, are advected from one grid point to another, while those along the diagonal directions, i.e., $c_{2,4,6,8}$, need to be interpolated after advection.

We consider the second-order central interpolation to set the "propagation" rules,

$$f_i(r_j) = a_- \tilde{f}_i(r_j - e_i) + a_0 \tilde{f}_i(r_j, t_n) + a_+ \tilde{f}_i(r_j + e_i), \tag{G2}$$

where $\tilde{f}_i$ denotes the postcollision value of f_i, e_i denotes the vector linking r_j to one of its neighboring lattice points along the direction of velocity c_i, and the interpolation coefficients for the axial and diagonal directions are, respectively, given by

$$a_- = \frac{1}{2}(r+1)r, \tag{G3a}$$

$$a_0 = (1+r)(1-r), \tag{G3b}$$

$$a_+ = \frac{1}{2}(r-1)r, \tag{G3c}$$

and

$$a_- = \frac{1}{4}(r+\sqrt{2})r, \tag{G4a}$$

$$a_0 = \frac{1}{2}(\sqrt{2}+r)(\sqrt{2}-r), \tag{G4b}$$

$$a_+ = \frac{1}{4}(r-\sqrt{2})r. \tag{G4c}$$

It should be noted that the above interpolation is only used as an example, and could easily be replaced by others, as, for instance, those used in Refs. [27–32].

For the octagonal velocity set, the transformation matrix M is

$$
\begin{pmatrix}
\langle \rho | \\
\langle j_x | \\
\langle j_y | \\
\langle p_{xx} | \\
\langle p_{xy} | \\
\langle e | \\
\langle q_x | \\
\langle q_y | \\
\langle \varepsilon |
\end{pmatrix}
=
\begin{pmatrix}
1 & 1 & 1 & 1 & 1 & 1 & 1 & 1 & 1 \\
0 & 1 & \varpi & 0 & -\varpi & -1 & -\varpi & 0 & \varpi \\
0 & 0 & \varpi & 1 & \varpi & 0 & -\varpi & -1 & -\varpi \\
0 & 1 & 0 & -1 & 0 & 1 & 0 & -1 & 0 \\
0 & 0 & 1 & 0 & -1 & 0 & 1 & 0 & -1 \\
-8 & 1 & 1 & 1 & 1 & 1 & 1 & 1 & 1 \\
0 & 1 & -\varpi & 0 & \varpi & -1 & \varpi & 0 & -\varpi \\
0 & 0 & -\varpi & 1 & -\varpi & 0 & \varpi & -1 & \varpi \\
0 & 1 & -1 & 1 & -1 & 1 & -1 & 1 & -1
\end{pmatrix},
\tag{G5}
$$

where $\varpi \equiv 1/\sqrt{2}$. The diagonal relaxation matrix is

$$S = \mathrm{diag}(0,0,0,s_{xx},s_{xy},s_e,s_q,s_q,s_\varepsilon), \tag{G6}$$

where we have set the relaxation rates for q_x and q_y to be equal.

The equilibria of the nonconserved moments are

$$p_{xx}^{(\mathrm{eq})} = \frac{1}{r}(j_x^2 - j_y^2), \tag{G7a}$$

$$p_{xy}^{(\mathrm{eq})} = \frac{2}{r}(j_x j_y), \tag{G7b}$$

$$e^{(\mathrm{eq})} = \alpha_2 \rho + \frac{9}{r}(j_x^2 + j_y^2), \tag{G7c}$$

$$q_{x,y}^{(\mathrm{eq})} = c_1 j_{x,y}, \tag{G7d}$$

$$\varepsilon^{(\mathrm{eq})} = \alpha_3 \rho + \gamma_4(j_x^2 + j_y^2). \tag{G7e}$$

For all practical purposes, we can set $\alpha_3 = \gamma_4 = 0$, as they have no effect on the hydrodynamic behavior of the system. In what follows, we shall set $\alpha_3 = 0$ and let γ_4 be a free parameter.
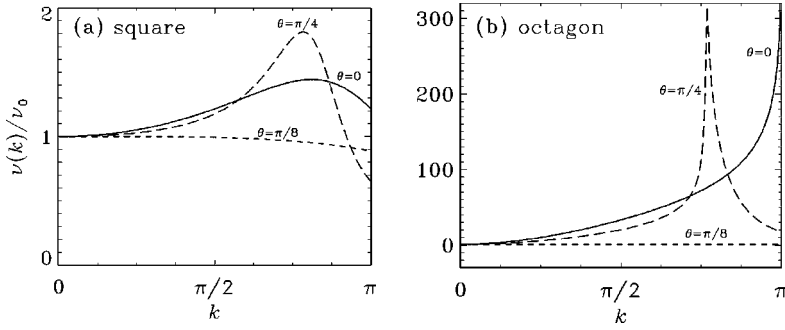
The isotropy of the shear viscosity [45] requires that

FIG. 5. The k dependence of the normalized viscosity, $\nu(\mathbf{k})/\nu_0$, for two LBGK models, with $\nu_0 = 0.001$. (a) The normal D2Q9 LBGK model on a 2D square lattice without interpolation and with $\tau = 0.503$. (b) The octagonal LBGK model with $r = 1$ and $\tau = 0.504$.

$$\left(\frac{1}{s_{xy}} - \frac{1}{2}\right) = \left(\frac{1 + c_1}{1 - c_1}\right)\left(\frac{1}{s_{xx}} - \frac{1}{2}\right). \qquad \text{(G8)}$$

Obviously, for the BGK models [27–32] to satisfy this condition, we must set $c_1 = 0$. The sound speed is

$$c_s = \frac{2r}{3}\sqrt{1 + \frac{\alpha_2}{8}} \qquad \text{(G9)}$$

and the shear and bulk viscosities are, respectively, given by

$$\nu = \frac{r^2}{4}(1 + c_1)\left(\frac{1}{s_{xx}} - \frac{1}{2}\right), \qquad \text{(G10)}$$

$$\zeta = \frac{r^2}{2}(1 - \theta_s)\left(\frac{1}{s_e} - \frac{1}{2}\right), \qquad \text{(G11)}$$

where $\theta_s = 2c_s^2/r^2 = (8 + \alpha_2)/9$. For the LBGK model, $c_1 = 0$ and $s_{xx} = s_e = 1/\tau$. The above results are obtained by the (linear) dispersion equation analysis and verified by the (nonlinear) Chapman-Enskog analysis plus some simulations in which one analyzes the relaxation of a flow with a periodic shear wave as initial condition.

The equilibrium distribution functions obtained from the equilibria of the moments are (assuming $\alpha_3 = 0$)

$$f_i^{(eq)} = \begin{cases} (1 - \theta_s)\rho - \dfrac{1}{r}\mathbf{j}\cdot\mathbf{j}, & i = 0 \\[2mm] \dfrac{1}{8}\left(\theta_s\rho + 2(\mathbf{c}_i\cdot\mathbf{j}) + \dfrac{1}{r}\{4(\mathbf{c}_i\cdot\mathbf{j})^2 - (2 - \gamma_4)\mathbf{j}\cdot\mathbf{j}\}\right), & i = 1,3,5,7 \\[2mm] \dfrac{1}{8}\left(\theta_s\rho + 2(\mathbf{c}_i\cdot\mathbf{j}) + \dfrac{1}{r}\{4(\mathbf{c}_i\cdot\mathbf{j})^2 - \gamma_4\mathbf{j}\cdot\mathbf{j}\}\right), & i = 2,4,6,8. \end{cases} \qquad \text{(G12)}$$

When $r = 1$, $c_s = 1/2$ ($\alpha_2 = -7/2$), and $\gamma_4 = 1$, the above equilibria reduce to that of the LBGK model,

$$f_i^{(eq)} = w_i\rho\{1 + 4\mathbf{c}_i\cdot\mathbf{u} + 8(\mathbf{c}_i\cdot\mathbf{u})^2 - 2\mathbf{u}^2\}, \qquad \text{(G13a)}$$

$$w_i = \begin{cases} 1/2, & i = 0, \\ 1/16, & i \neq 0, \end{cases} \qquad \text{(G13b)}$$

which are derived from the Maxwellian [42,43].

The analysis of the dispersion equation (cf. Appendix B and Ref. [45]) shows the non-hydrodynamic effects due to the discreteness of the LBE system, i.e., the small spatial scale behaviors of the system. Here we shall only show the k dependence of the shear viscosity ν. Figure 5 shows the $\nu(\mathbf{k})/\nu_0$ along three directions: $\theta = 0$, $\pi/8$ (22.5°), and $\pi/4$ (45°), where θ is the polar angle of $\mathbf{k}$, and ν_0 is the viscosity
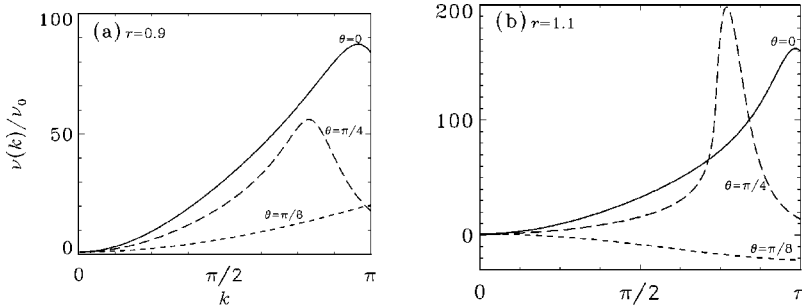

FIG. 6. The k dependence of the normalized viscosity, $\nu(\mathbf{k})/\nu_0$, for the octagonal BGK model, with $\nu_0 = 0.001$ and $r \neq 1$. (a) $r = 0.9$ and $\tau \approx 0.504\,94$. (b) $r = 1.1$ and $\tau \approx 0.503\,31$.

at $k=0$ as given by Eq. (G10). Figures 5(a) and 5(b) illustrate the behavior of $\nu(k)/\nu_0$ for the usual D2Q9 LBGK model on a 2D square lattice and the 2D nine-velocity octagonal model with interpolations along diagonal directions ($r=1$), respectively. Clearly, the use of octagonal velocity set does not improve the isotropy. To the contrary, the octagonal model displays a much larger $[O(10^2)]$ anisotropic effect in $\nu(k)/\nu_0$ than its counterpart on a 2D square lattice. Because the octagonal model has much larger numerical viscosities, it is much less sensitive to disturbances of small scales, thus much more stable numerically. In particular, since the value of $\nu(k)/\nu_0$ for the octagonal model reaches its maximum at $k=\pi$ along the lattice lines ($\theta=0$), the model is not sensitive to the spurious staggered mode (i.e., the checkerboard pattern of wavelength 2). We also compute $\nu(k)/\nu_0$ for the octagonal LBGK model with $r\neq1$ or $r\neq\sqrt{2}$, i.e., with interpolations applied to all eight directions. Figures 6(a) and 6(b) show the behavior of $\nu(k)/\nu_0$ for the 2D nine-velocity octagonal model with interpolations applied to all eight directions, and for $r=0.9$ and $r=1.1$, respectively. Similar to the case of $r=1$, the octagonal model displays large anisotropy when interpolations are applied to all eight directions ($r\neq1$ or $r\neq\sqrt{2}$). It should be noted that Fig. 6(b) shows the case that the octagonal model has become linearly unstable along the direction of $\theta=\pi/8$ because $\nu(k)$ becomes negative in a wide range of k. Based on these results, we conclude that, when compared to the LBGK model without interpolation, the octagonal LBGK model is much more anisotropic and has much larger numerical viscosities due to interpolations. Thus, the interpolations which are less symmetric than the velocity set can easily destroy the symmetry properties brought by the velocity set and, in turn, dictate the symmetry properties of the model as a whole. To fully retain the symmetry of the velocity set, the interpolations with a comparable symmetry may have to be used (with a compromise between anisotropy and nonhydrodynamical behavior).

The limitation of the LBGK model becomes apparent in this analysis. First, the LBGK model has much narrower stable ranges of adjustable parameters when compared to the MRT counterpart, as shown in Ref. [45]. For example, with the MRT models one can properly maintain a suitable ratio between the bulk and shear viscosities to help stabilize the system by reducing undesirable acoustic effects. This is particularly useful when using poor initial conditions leading to
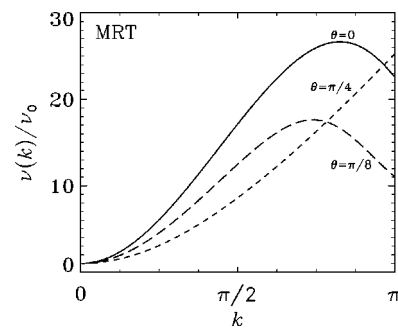

FIG. 7. The k dependence of the normalized viscosity, $\nu(k)/\nu_0$, for the octagonal MRT model, with $\nu_0=0.001$. Other parameter values are $c_1=0.4$, $\alpha_2=-6$, $\alpha_3=0$, $s_e=1.60$, $s_q=1.84$, $r=0.6$, and $s_{xx}=1.96875$.

large acoustic disturbance. Second, it is not possible for the LBGK model to incorporate the stretching factor r into the equilibria *a priori*. It can be shown that the octagonal LBGK model would not be able to maintain the Galilean invariance for $r\neq1$. And third, the LBGK models do not have the flexibility to optimize certain properties. In contrast, the MRT models have the freedom and capability to optimize certain properties. As an example, Fig. 7 shows $\nu(k)/\nu_0$ for the MRT model with the octagonal velocity set. It is obvious that the anisotropy of $\nu(k)/\nu_0$ at large k is much reduced.

Finally, we would like to mention that we have also analyzed a more elaborate LBGK model on a 2D octagonal lattice with three speeds (0, 1, and 2) and 17 velocities [27]. Our observation can be summarized as follows. First, the addition of a second velocity set (of speed 2) does not improve the isotropy of the system. And second, when the energy-conservation constraint is imposed, the model displays exactly the same spurious coupling between the energy and shear modes, as shown in Sec. III C and Fig. 2. This coupling strongly depends on the Prandtl number Pr. In particular, the value of k_c at which the spurious coalescence occurs (cf. Sec. III C) decreases as $|{\rm Pr}-1|$ decreases. This poses a severe limitation on the energy-conserving LBE models because for many fluids of practical interest the Prandtl number is close to 1 (e.g., Pr$\approx$0.71 for air). We also observe that the D2Q17 MRT model with octagonal velocities has sufficiently large stable ranges of the sound speed c_s, the viscosity ν, and the thermal conductivity κ. The details of this analysis shall be published elsewhere.

[1] D. d'Humières, Prog. Astronaut. Aeronaut. **159**, 450 (1992).

[2] F. Massaioli, R. Benzi, and S. Succi, Europhys. Lett. **21**, 305 (1993).

[3] J.G.M. Eggels and J.A. Sommers, Int. J. Heat Fluid Flow **16**, 357 (1995).

[4] X. Shan, Phys. Rev. E **55**, 2780 (1997).

[5] R.G.M. van der Sman, M.H. Ernst, and A.C. Berkenbosch, Int. J. Heat Mass Transfer **43**, 577 (2000).

[6] S. Succi, G. Bella, and F. Papetti, J. Sci. Comput. **12**, 395 (1997).

[7] G. Yan, Y. Chen, and S. Hu, Phys. Rev. E **59**, 454 (1999).

[8] F.L. Hinton, M.N. Rosenbluth, S.K. Wong, Y.R. Lin-Liu, and R.L. Miller, Phys. Rev. E **63**, 061212 (2001).

[9] W. Shi, W. Shyy, and R. Mei, Numer. Heat Transfer, Part B **40**, 1 (2001).

[10] J. Huang, F. Xu, M. Vallieres, D.H. Feng, Y.H. Qian, B. Fryxell, and M.R. Strayer, Int. J. Mod. Phys. C **8**, 827 (1997).

[11] A. Renda, G. Bella, S. Succi, and I.V. Karlin, Europhys. Lett. **41**, 279 (1998).

[12] C. Sun, Phys. Rev. E **58**, 7283 (1998).

[13] C. Sun, Phys. Rev. E **61**, 2645 (2000).

[14] C. Sun, J. Comput. Phys. **161**, 70 (2000).

[15] R.J. Mason, J. Stat. Phys. **107**, 385 (2002).

[16] F.J. Alexander, S. Chen, and J.D. Sterling, Phys. Rev. E **47**, R2249 (1993).

[17] Y.H. Qian, J. Sci. Comput. **8**, 231 (1993).

[18] G. McNamara and B.J. Alder, Physica A **194**, 218 (1993).

[19] Y. Chen, H. Ohashi, and M. Akiyama, Phys. Rev. E **50**, 2776 (1994).

[20] G. McNamara, A. Garcia, and B.J. Alder, J. Stat. Phys. **81**, 395 (1995).

[21] G. McNamara, A. Garcia, and B.J. Alder, J. Stat. Phys. **87**, 1111 (1997).

[22] X. He, S. Chen, and G.D. Doolen, J. Comput. Phys. **146**, 282 (1998).

[23] B.J. Palmer and D.R. Rector, J. Comput. Phys. **161**, 1 (2000).

[24] B.J. Palmer and D.R. Rector, Phys. Rev. E **61**, 5295 (2000).

[25] T. Ihle and D.M. Kroll, Comput. Phys. Commun. **129**, 1 (2000).

[26] T. Inamuro, Philos. Trans. R. Soc. London, Ser. A **360**, 477 (2002).

[27] P. Pavlo, G. Vahala, and L. Vahala, Phys. Rev. Lett. **80**, 3960 (1998).

[28] P. Pavlo, G. Vahala, L. Vahala, and M. Soe, J. Comput. Phys. **139**, 79 (1998).

[29] M. Soe, G. Vahala, P. Pavlo, L. Vahala, and H. Chen, Phys. Rev. E **57**, 4227 (1998).

[30] G. Vahala, P. Pavlo, L. Vahala, and M.S. Martys, Int. J. Mod. Phys. C **9**, 1247 (1998).

[31] L. Vahala, D. Wah, G. Vahala, J. Carter, and P. Pavlo, Phys. Rev. E **62**, 507 (2000).

[32] P. Pavlo, G. Vahala, and L. Vahala, J. Stat. Phys. **107**, 499 (2002).

[33] O. Filippova and D. Hänel, Int. J. Mod. Phys. C **9**, 1439 (1998).

[34] O. Filippova and D. Hänel, J. Comput. Phys. **158**, 139 (2000).

[35] Z. Guo, B. Shi, and C. Zheng, Int. J. Numer. Methods Fluids **39**, 325 (2002).

[36] M. De Cicco, S. Succi, and G. Bella, SIAM J. Sci. Comput. (USA) **21**, 366 (1999).

[37] B.T. Nadiga, J. Stat. Phys. **81**, 129 (1995).

[38] R.H. Sanders and K.H. Prendergast, Astrophys. J. **188**, 489 (1974).

[39] K. Xu and L.-S. Luo, Int. J. Mod. Phys. C **9**, 1177 (1998).

[40] K. Xu, *Gas-kinetic Schemes for Unsteady Compressible Flow Simulations*, Von Karman Institute Lecture Series Vol. 1998-03 (Von Karman Institute, Brussels, 1998).

[41] K. Xu, J. Comput. Phys. **171**, 289 (2001).

[42] X. He and L.-S. Luo, Phys. Rev. E **55**, R6333 (1997).

[43] X. He and L.-S. Luo, Phys. Rev. E **56**, 6811 (1997).

[44] X. Shan and X. He, Phys. Rev. Lett. **80**, 65 (1998).

[45] P. Lallemand and L.-S. Luo, Phys. Rev. E **61**, 6546 (2000).

[46] The ability of the scheme proposed in Ref. [32] may be ques-
tioned in view of the results shown in Fig. 1(c) of Ref. [32]. In the 2D Poiseuille flow, the measured viscosity ν is always larger than the theoretical value ν_0 and is strongly channel width dependent (for a channel width $H = 10$, $\nu \approx 3\nu_0$). This is not the case for the usual LBE schemes in which the viscosity ν can be very accurately determined analytically, provided boundary conditions are properly dealt with [48].

[47] Y. Peng, C. Shu, and Y.T. Chew, Phys. Rev. E **68**, 026701 (2003).

[48] D. d'Humières and I. Ginzburg, ITWM Report No. 38-2002 (unpublished); see http://www.itwm.fhg.de

[49] D. d'Humières, M. Bouzidi, and P. Lallemand, Phys. Rev. E **63**, 066702 (2001).

[50] D. d'Humières, I. Ginzburg, M. Krafcyzk, P. Lallemand, and L.-S. Luo, Proc. R. Soc. London, Ser. A **360**, 437 (2002).

[51] P.L. Bhatnagar, E. P Gross, and M. Krook, Phys. Rev. **94**, 511 (1954).

[52] M. Bouzidi, D. d'Humieres, P. Lallemand, and L.-S. Luo, J. Comput. Phys. **172**, 704 (2001).

[53] We regret that there are typos made in Eqs. (16e) and (16f) in our previous paper [45]. Although the formulas are correct, the numerical factor in Eqs. (16e) and (16f) should be 3/2, instead of 1/2.

[54] Y.H. Qian and Y. Zhou, Europhys. Lett. **42**, 359 (1998).

[55] P. Grosfils and P. Lallemand, Europhys. Lett. **24**, 473 (1993).

[56] D. Dubbeldam, A.G. Hoekstra, and P.M.A. Sloot, Comput. Phys. Commun. **129**, 13 (2000).

[57] P.A. Skordos, Phys. Rev. E **48**, 4823 (1993).

[58] L.D. Landau and E.M. Lifshitz, *Fluid Mechanics*, 2nd ed. (Pergamon Press, Oxford, 1987).

[59] I.G. Currie, *Fundamental Mechanics of Fluids*, 2nd ed. (McGraw-Hill, Boston, 1993).

[60] M. Junk and A. Klar, SIAM J. Sci. Comput. (USA) **22**, 1 (2000).

[61] M. Junk, Numer. Methods Partial Differ. Equ. **17**, 383 (2001).

[62] M. Hénon, Complex Syst. **1**, 763 (1987).

[63] I. Ginzburg and P.M. Adler, J. Phys. II **4**, 191 (1994).

[64] Z. Guo, C. Zheng, and B. Shi, Phys. Rev. E **65**, 046308 (2002).

[65] D. d'Humières (private communication).

[66] E. Tric, G. Labrosse, and M. Betrouni, Int. J. Heat Mass Transfer **43**, 4043 (2000).

[67] A. Mezrhab, M. Bouzidi, and P. Lallemand, Comput. Fluids (to be published).

[68] J.O. Hirschfelder, C.F. Curtiss, and R.B. Bird, *Molecular Theory of Gases Liquids* (Wiley, New York, 1954).

[69] L.-S. Luo and S.S. Girimaji, Phys. Rev. E **66**, 035301(R) (2002).

[70] L. Giraud, D. d'Humières, and P. Lallemand, Europhys. Lett. **42**, 625 (1998).

[71] P. Lallemand, D. d'Humières, L.-S. Luo, and R. Rubinstein, Phys. Rev. E **67**, 021203 (2003).

[72] L.-S. Luo, H. Chen, S. Chen, G.D. Doolen, and Y.C. Lee, Phys. Rev. A **43**, 7097 (1991).